Master's Thesis – Master Earth Surface and Water

Projections of Land Loss to Major Deltas: The Effects of Relative Sea-Level Rise and Fluvial Sediment Delivery in the 21st Century

Author

Briangga Herswastio Bromo
1622765

Supervisors

Dr. ir. Jaap Nienhuis & Dr. Frances Dunn
Department of Physical Geography

2024

Abstract

River deltas are currently at risk of substantial land loss due to the dual threats of RSLR and declining fluvial sediment supply. Here we use IPCC RSLR scenarios and projections of fluvial sediment supply to build a model of delta response for 47 world's major delta. We model 9 scenarios representing four climate pathways (Representative Concentration Pathways 2.6, 4.5, and 8.5), three socioeconomic pathways (Shared Socioeconomic Pathways 1, 2, and 3), and one dam construction timeline. The model results indicate that 35 out of 47 deltas are expected to undergo a loss in the delta area by the end of the 21st century, considering the average scenario. The potential loss for the total of 47 major deltas ranges from 4,924.57 km2 for SSP 3, RCP 2.6 scenarios to 18,161.18 km2 for SSP 1, RCP 8.5 scenarios. The largest projected delta area change suggests a potential 2.78% area loss for the total of 47 major deltas. These anticipated area losses are primarily driven by the overwhelming impact of climate change-induced sea-level rise compared to the combined effects of anthropogenic activities (socio-economic factors and dam construction) and climate-change-induced fluvial sediment delivery. Notably, concerning the fluvial sediment delivery effect on relative delta area change, we find that anthropogenic activities (socio-economic and dam construction) appear to have a more significant impact on the reduction in the changes of delta area rate over time than the effect of future climate change.

Acknowledgement

I would like to express my heartfelt gratitude to everyone who contributed to this project. Firstly, I am deeply thankful to my academic supervisors, Dr. ir. Jaap Nienhuis and Dr. Frances Dunn, for their unwavering guidance and encouragement throughout this endeavor. Despite my initial challenges and limitations in understanding, their expertise and enthusiasm provided invaluable insights and helped alleviate my uncertainties. I am truly grateful for their support, which enabled me to gain new perspectives and make significant progress.

I also extend my appreciation to my project teammate, Astrid Hooijmans. Our collaboration allowed us to stay on track and support each other, fostering a productive and enriching environment for our work. I am grateful for Astrid's contributions and dedication, which undoubtedly enhanced the quality of our project.

Lastly, but certainly not least, I want to express my deepest gratitude to my family in Indonesia. Their unwavering support and encouragement have been a constant source of strength and motivation throughout this journey. Their belief in me has been instrumental in overcoming challenges and achieving milestones. I am truly blessed to have such a supportive and loving family by my side.

Content

List of Figures

1 Introduction

1.1 River Delta

Deltas serve as the habitat for approximately 500 million people worldwide, representing a vital and expanding population centre at the intersection of rivers and oceans (Tessler et al., 2015; Higgins, 2016). Additionally, the strategic and productive nature of coastal deltaic regions makes them global hotspots for economic activities, agriculture, aquaculture, and transportation, attracting significant human settlement. Furthermore, delta areas contribute to essential ecological features such as wetlands, mangrove forests, and ecological reserves, establishing them as crucial hubs for both economic and environmental functions on Earth (Higgins, 2016; Edmonds et al., 2020).

Deltas formed through the dynamics of the relative sea-level rise (RSLR) and the fluvial sediment delivery (Ericson et al., 2006). These dynamics allow the delta shoreline to advance seaward through surplus fluvial sediment delivery and retreat landward through the relative sea-level rise. Investigation has been performed and validated for these dynamics through field observation (Helland-Hansen and Martinsen, 1966; Blum and Törnqvist, 2000), experiment (Muto, 2001; Kim et al., 2006, 2009; Lai and Capart, 2009), and numerical modelling (Swenson, 2005; Fagherazzi and Overeem, 2007; Hoogendoorn et al., 2008; Anderson et al., 2019). These roles of RSLR and sediment supply can be estimated to find the shoreline equilibrium by the following equation (Nienhuis et al., 2023):

$$Q_{river} \cdot f_r = \dot{S} \cdot A_{delta}$$

Equation 1

Where Q_{river} is the rate of sediment supply (m^3/year) that is retained on the delta (f_r, between 0 and 1) is equivalent to the rate of relative sea-level rise ($\dot{S}$, m/year) across the delta surface area (A_{delta}, m^2) which is the sum of the delta topset area (A_{topset}, m^2) and the delta foreset area ($A_{foreset}$,m^2). This equation was used in the most basic 2D model with the assumption of a constant width. Following the above approximation, the projection of the delta will remain the same as the current condition if, in the future, the equation is in equilibrium. However, the shoreline will migrate seaward (regression or progradation) or landward (transgression or retrogradation) if the equation deviates from the balance depending on which factors will affect more to the deltas as can be seen in Figure 1.1 (Nienhuis et al., 2023).

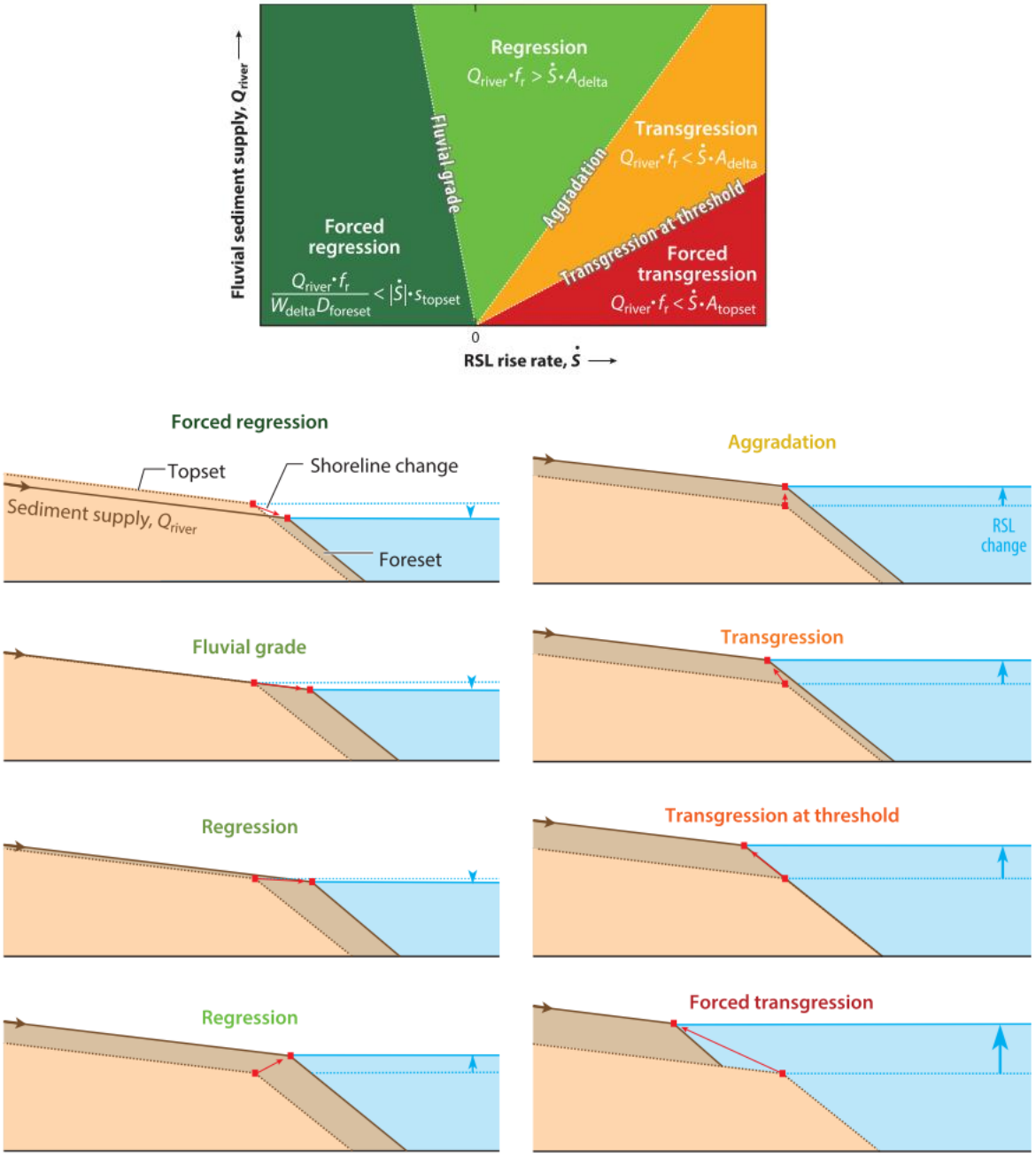

Figure 1.1 The process of shoreline migration in response to the RSL and sediment supply. Source: Nienhuis et al. (2023).

At present, low-lying land areas like river deltas are particularly vulnerable to the threat of RSLR and are likely to be inundated by the end of the century (Ericson et al., 2006; Syvitski et al., 2009). The resilience of topset delta areas against RSLR relies on frequent inundation, facilitating sediment deposition that elevates the delta to sea level through a process known as aggradation.

Consequently, deltas exhibit a natural resistance to RSLR owing to this mechanism (Ibáñez et al., 2014).

However, the substantial population growth in deltaic regions over recent centuries has made anthropogenic activities a predominant influence on aggradation (Mcmanus, 2002; Syvitski, 2008; Syvitski and Kettner, 2011). Research indicates that these human-induced activities tend to diminish the impact of aggradation (Syvitski et al., 2009) Despite the dual challenges of RSLR and anthropogenic effects, previous research shows that the global delta lands have experienced a net land gain for the last 30 years, considerably driven by human activity-induced surplus sediment flux (Nienhuis et al., 2020). Therefore, it becomes imperative to investigate the balance between sediment flux and RSLR as a pivotal determinant of delta geomorphology (Giosan et al., 2014).

1.2 The Influence of RSLR and Fluvial Sediment Delivery on Future Delta

1.2.1 Relative Sea-level Rise (RSLR)

Global delta areas are confronted with the challenges posed by sea-level rise and global climate change. Moreover, at the regional level, there is a compounded impact resulting from the combined effects of sea-level rise and vertical land movement (VLM), collectively referred to as relative sea-level rise (RSLR) (Nicholls and Cazenave, 2010; Hinkel et al., 2014; Tessler et al., 2018).

1.2.1.1 Sea-level rise

At present, river deltas globally face an impending risk of inundation, potentially affecting an estimated population of 176 to 287 million individuals under the RCP 8.5 scenario in 2100 (Kirezci et al., 2020). Moreover, the research shows an increase of global delta area at risk by 48% by 2100 compared with the present day. The phenomenon of sea-level rise significantly contributes to the heightened vulnerability of riverine areas to flooding, as avulsion events migrate upstream, thereby exposing an expanded population to potential threats (Li et al., 2022). Some deltas, lacking sustainable protections, face considerable impacts; for example, the Mississippi and Rhine deltas may experience four to eight times higher relative risk under the threat of flooding, while the Chao Phraya and Yangtze deltas could encounter a one-and-a-half to four times higher relative risk (Tessler et al., 2018).

The assessment conducted by the Intergovernmental Panel on Climate Change (IPCC) (Oppenheimer et al., 2019) reveals that the rate of sea-level rise (SLR) has increased nearly threefold, from 1.4 mm/yr to 3.6 mm/yr, since the early 20th century. Projections from the IPCC indicate that the global mean sea level (GMSL) is anticipated to rise between 0.43 m and 0.84 m by 2100 relative to the period 1986–2005, under the lowest (RCP 2.6) and highest (RCP 8.5) scenarios, respectively. In addition, the RSL rate in 2100 will reach 15 mm/yr under RCP 8.5, which means around 2.5 times higher than the current rate. Furthermore, the RSL rate in 2100 is

projected to reach 15 mm/yr under RCP 8.5, representing approximately 2.5 times the current rate. It's crucial to note that sea-level rise is not uniformly distributed globally, and the variations in regional sea levels have significant implications for coastal communities worldwide (Nicholls, 2011; Kopp et al., 2015; Woodworth et al., 2019).

Sea levels in the world exhibit variations due to various drivers originating from processes with both local and distant impacts on deltas (Gregory et al., 2019; Hamlington et al., 2020). These drivers include temperature and salinity variations, which affect water volume (steric sea-level change); changes in the amounts of water in the ocean from glaciers, ice sheets, and land water storage (barystatic sea-level change); and the influence of ocean circulation (ocean dynamic effect) along with changes in gravitational field, Earth rotation, and solid Earth deformation (Nienhuis et al., 2023). These processes collectively contribute to sea-level changes, with their effects considerably surpassing those directly caused by local deltaic processes. Figure 1.2 illustrates variations in sea level across different locations worldwide.

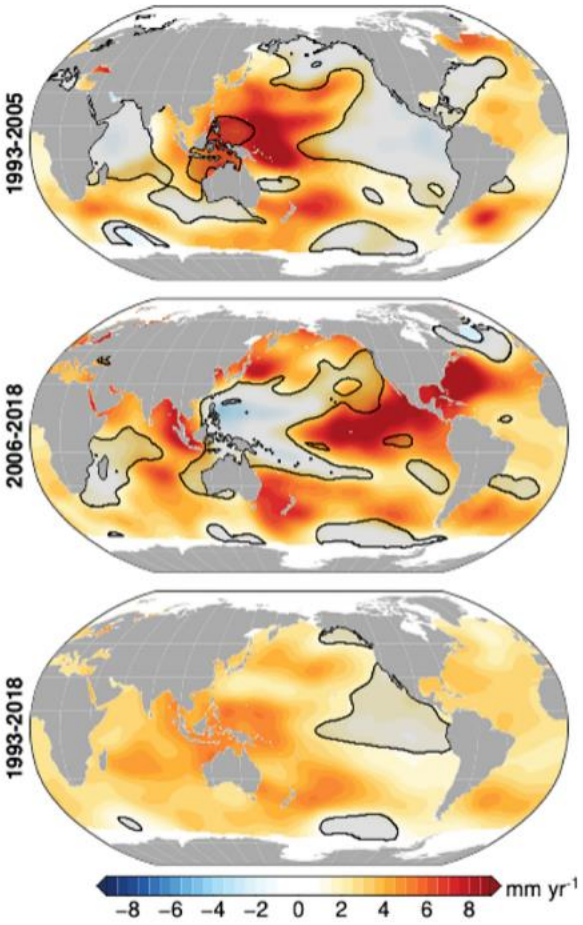

Figure 1.2 Satelite altimeter-measured regional sea-level trend patterns from (top) 1993 – 2005, (middle) 2006 – 2018, (bottom) 1993 – 2018. Source: Hamlington et al. (2020).

1.2.1.2 Vertical Land Movement (VLM)

Along with, sea-level change, the vertical land movement (VLM) affects changes in deltaic land area. The combination of those effects is jointly referred to as relative sea level (RSL). VLM is classified as a contribution of several processes, such as (a) tectonic movement, (b) isostatic adjustment, (c) fluid extraction, and (d) sediment compaction and oxidation. Notably, this study excludes sedimentation and erosion from the definition of VLM. However, it is apparent that some studies include these mechanisms, such as Tessler et al. (2018).

Large deltas undergo greater VLM than non-deltaic zones due to natural processes and human activities (Biljsma et al., 1995; Erban et al., 2014). Shallow processes, such as sediment compaction, show spatial variability and rapid effects (e.g., Nienhuis et al., 2017), while deeper processes, like lithospheric flexure, have slower, wide-ranging impacts (Yu et al., 2012; Wolstencroft et al., 2014; Kuchar et al., 2018).

1.2.2 Fluvial Sediment Delivery

Equally important, the insufficiency in fluvial sediment transport exacerbates the situation, as it hinders the capacity to elevate the delta landform. Previous research shows that 92% of people exposed to tropical activities live in the delta with a deficit fluvial sediment flux (Edmonds et al., 2020).

To sustain the equilibrium of delta geomorphology, it is important to ensure an adequate supply of fluvial sediment (refer to 1.1). However, research indicates that 33 out of 47 major deltas worldwide will confront a decline in sediment flux by the year 2100, with reductions reaching up to 83% (Figure 1.3) (Dunn et al., 2019). These declines are attributed to both anthropogenic activities and the future of climate change. Furthermore, the construction of upstream dams has become a recurring challenge for many of the world's major deltas, contributing to diminished fluvial sediment transport to deltaic regions(Syvitski et al., 2005, 2009).

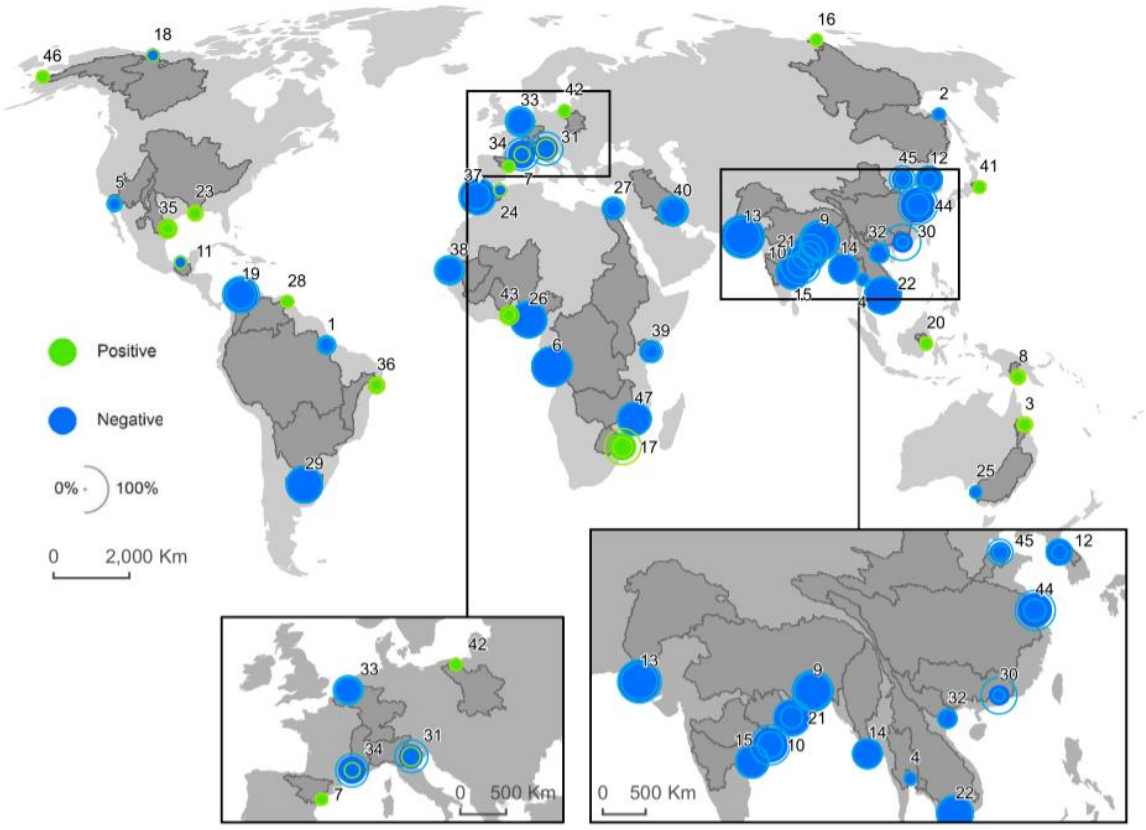

Figure 1.3 Projected percentage change in simulated mean annual fluvial sediment flux between 1990 – 2019 and 2070 – 2099 for 47 major deltas. The green (increase in sediment flux) and blue (decrease in sediment flux) circles are scaled to represent the mean annual. Source: Dunn et al. (2019)

1.3 The Development of Future Projections

A widely used and simpler model, often referred to as the "bathtub" or passive flood model, is commonly employed for projecting future deltas. This model is favoured for its ease of use and lack of complexity in modelling, providing the necessary spatial specificity (Anderson et al., 2018). However, the "bathtub" or passive flood model typically assumes a uniform rise in water levels, neglecting crucial factors such as river discharges, sedimentation, and erosion. These oversights can lead to significant discrepancies in the predicted outcomes (Anderson et al., 2018; Juhász et al., 2023).

To address these limitations, the true coastal change method has been proposed. Research conducted by Nienhuis et al. (2020) utilizes this method, predicting delta morphology and changes in delta morphology by calculating sediment transport fluxes driven by waves, tides, and rivers. In comparison to the simplistic estimations of the bathtub model, the true coastal change

method reveals that deltas have experienced land gains in recent decades despite the presence of sea-level rise.

Recent studies have adopted the true coastal change method, employing a simple morphodynamic model to project global delta area changes in the 21st century. This projection, conducted by Nienhuis and van de Wal (2021), involves a comparison of sediment supply against RSLR. The datasets utilized include projections of sea-level rise from the IPCC (Oppenheimer et al., 2019) and modern fluvial sediment supply retrieved from WBMSed (Cohen et al., 2014; Nienhuis et al., 2020).

Nonetheless, in the scope of this study, it is important to note that, within the scope of this study, the measurement of sediment flux is held constant, simulating present-day conditions. It is acknowledged that such conditions are unlikely to remain static in future scenarios (see 1.2.2), introducing a potential source of uncertainty in the projections.

Therefore, to enhance the significance of fluvial sediment delivery in comparison to sea-level rise projections, the fluvial sediment delivery projections provided by Dunn (2019) are incorporated. As a result, the contribution of each component will be calculated over the years to predict the change of the delta area in the future. Consequently, the contribution of each component will be assessed over time to predict changes in the delta area in the future. This approach aims to provide a more comprehensive understanding of delta processes, considering both sediment delivery and relative sea-level rise components.

1.4 Hypothesis

This thesis builds upon prior research conducted by Nienhuis and van de Wal (2021), which leveraged the fluvial sediment supply projections from Dunn (2019) to improve the model. Therefore, this research hypothesizes that the expected decline in fluvial sediment delivery by the year 2100 is expected to play a pivotal role in the reduction of global delta areas, complemented by the concurrent rise in sea levels. Other than that, the intricacies of the interaction between declining sediment delivery and rising sea levels are projected to yield diverse outcomes across various deltas, introducing variations in the patterns of delta area changes.

1.5 Aim and Outline of the Research

The study aims to achieve two primary objectives: (1) To project land area changes in the 21st century for 47 of the world's major deltas and (2) To identify the principal factors driving alterations in deltaic land area. For this purpose, the following research questions need to be answered:

1. **How will the land areas of the 47 major deltas change in response to the climatic and socio-economic conditions during the 21st century?**
2. **Which contributing factors influence changes in land area within these 47 major deltas?**
   - Is the variation in the delta area primarily attributed to fluvial processes or sea-level rise dynamics?
   - To what extent can the principal driving factors impact alterations in the deltaic land area?

2 Methods

2.1 Study Area

2.1.1 Selected Delta Areas and the Surface Area.

The dataset utilized for the model originates from Ericson et al. (2006), which builds upon previous work by Tessler et al. (2015). These studies focus on 47 major deltas, chosen to represent a diverse range of climates, geomorphologies, population densities, and socio-economic conditions. The geographic locations of the river mouths for these deltas are illustrated in Figure 2.1, and their delta surface area and delta foreset depth are listed in Table 2-1.

To understand the changes in the delta areas, it is essential to learn the A_{delta} in the initial year (2007). Initially, the total A_{delta} for the 47 major deltas in 2007 is reported as 652,281 km^2. Table 2-1 shows the distribution of the delta area for all deltas. Notably, the Amazon Delta and Ganges Brahmaputra Meghna (GBM) Delta emerge as the largest deltas, exhibiting a substantial disparity compared to other deltas. Together, these two deltas account for 30.88% of the total delta area.

Additionally, the ten largest deltas collectively contribute to almost 70% of the total A_{delta} for the 47 major deltas. To see the disparity of the A_{delta}, the ten largest deltas along with their corresponding A_{delta} are presented in Table 2-1. As per the table, it is observed that The Mekong Delta, ranked as the third-largest delta, is approximately half the size of the Amazon Delta. The disparity indicates a significant difference in the magnitudes of these two major deltas. Afterwards, there is a notable difference between the Mekong Delta and the fourth-largest delta, the Yangtze Delta, followed by a more consistent and relatively small difference. The fact that these ten deltas contribute to 70% of the total A_{delta} indicates the dominance of these larger deltas, while the remaining deltas constitute relatively small areas.

Table 2-1 Names, delta surface areas (A_{delta}, km^2), and delta foreset depth (D_f , m) for the 47 major deltas sorted from the largest delta to the smallest delta

Delta Name	Delta Area (km^2)	Delta Foreset Depth (m)
Amazon	109,000	50.00
Ganges Brahmaputra Meghna	92,455	41.27
Mekong	50,713	50.00
Yangtze	36,776	22.58
Irrawaddy	33,212	31.27
Mississippi	29,068	15.91
Nile	27,842	13.23
Orinoco	26,833	31.70
Chao Phraya	23,707	11.45
Lena	20,197	12.32
Niger	18,681	21.94
Rio Grande	15,845	13.83

Parana	15,263	19.03
Mackenzie	13,153	12.06
Zambezi	12,567	25.66
Mahanadi Brahmani Baiterani	12,448	16.58
Pearl	11,569	24.31
Grijalva	11,514	12.02
Colorado	8,611	14.72
Yellow	6,391	9.84
Indus	5,809	28.16
Red	5,704	13.94
Mahakam	5,569	21.20
Yukon	5,453	16.08
Rhine	4,821	17.43
Tigris Euphrates	4,734	12.95
Senegal	4,554	14.72
Magdalena	4,131	23.15
Godavari	3,996	14.87
Fly	3,541	13.65
Limpopo	3,412	19.91
Volta	2,916	14.47
Vistula	2,638	11.96
Han	2,536	5.42
Krishna	2,433	13.03
Congo	2,219	34.93
Murray	2,076	3.79
Rhône	1,683	6.43
Amur	1,452	14.05
São Francisco	1,311	18.35
Burdekin	1,241	10.16
Tone	1,026	21.13
Po	948	7.65
Tana	919	17.08
Ebro	539	7.87
Moulouya	530	10.04
Sebou	245	18.67

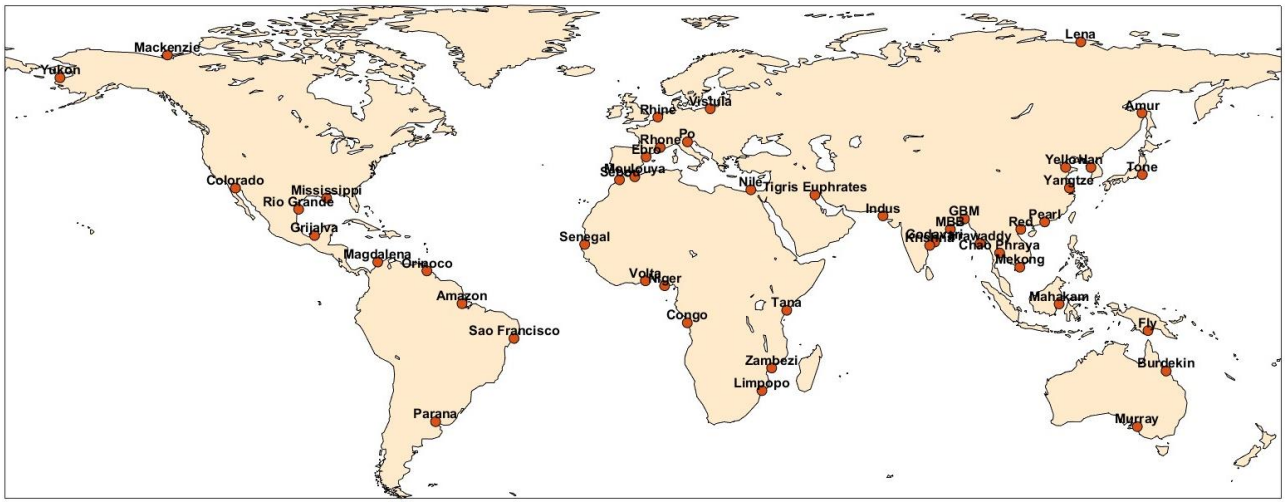

Figure 2.1 Geographic locations of the river mouths for the 47 major deltas used in this model.

2.1.2 The Retrieval of Delta Foreset Depth

The Delta foreset depth (D_f) in this research is obtained from Nienhuis and van de Wal (2021). To obtain the D_f, both subaerial and subaqueous delta profiles were obtained from the global SRTM15+ elevation dataset (Tozer et al., 2019). The $D_{foreset}$ is extracted from the elevation profile by selecting the deepest basement slope that extends the subaerial (between 0 and 30 m elevation) and subaqueous (between 0 and -40 m water depth) elevations. Next, the result must take into account that the delta depth must exceed the channel depth. the $D_{foreset}$ can be seen as h_b in Figure 2.2.

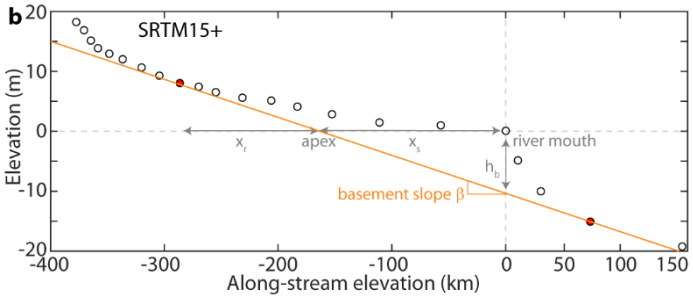

Figure 2.2 Elevation along the fluvial and offshore profile, including estimated delta length, apex, and delta depth.

2.2 Model Components and Input Datasets

2.2.1 A Model of Delta Area Change

A morpho-kinematic approach proposed by Wolinsky (2009) is employed to quantify the changes in delta surface area. The calculation relies on the equilibrium between the sedimentation, which tends to drive shoreline seaward, and sea-level rise, which tends to drive shoreline landward. The approach presupposes the balance of the shoreface profile while morphology is constant through time. The calculation is expressed as

$$H_s \frac{ds}{dt} = {c_0}^{-1}\Delta_q \ - L \cdot R$$

Equation 2

Afterwards, the notations from Wolinsky (2009) were converted by Nienhuis and van de Wal (2021) to align with the delta dataset as follows,

$$D_f \frac{dl_{delta}}{dt} = \frac{f_r \cdot Q_{river}}{w_{delta}} \ - l_{delta} \cdot RSLR$$

Equation 3

which H_s is delta foreset depth (D_f), s is the length of the delta from apex to mouth (l_{delta}), ${c_0}^{-1}\Delta_q$ is the width-averaged sediment supply ($f_r \cdot Q_{river}/w_{delta}$), L is the length of the delta (l_{delta}), and R is the relative sea-level rise (RSLR). Afterwads, multiplying both sides with w_{delta},

$$w_{delta} \cdot D_f \frac{dl_{delta}}{dt} = \ w_{delta} \cdot \frac{f_r \cdot Q_{river}}{w_{delta}} \ - w_{delta} \cdot l_{delta} \cdot RSLR$$

Equation 4

Rewriting the equation to accommodate delta area prediction by using $A_{delta} = \ w_{delta} \cdot l_{delta}$, thus the calculation is expressed as follows,

$$\frac{dA_{delta}}{dt} = \frac{Q_{river} \,.\, f_r - A_{delta} \,.\, RSLR}{D_{foreset}}$$

Equation 5

Where A_{delta} is the river delta area (m^2), dA_{delta}/dt is the changing of the delta area over time (m^2/year).

2.2.2 Relative Sea-level Rise

The sea-level data is based on the climate-change-driven estimation for various Representative Concentration Pathway (RCP) scenarios, as outlined in the Intergovernmental Panel on Climate Change (IPCC) Special Report on the Ocean and Cryosphere in a Changing Climate (SROCC) by Oppenheimer et al. (2019). The future RSLR (2007-2100) was extracted for RCP 2.6, 4.5, and 8.5 by finding the nearest data for each delta from the 1-degree grid.

In addition, the vertical land movement (VLM) was determined using data from GPS and tide gauges (Pfeffer and Allemand, 2016; Blewitt et al., 2018; Shirzaei et al., 2021). VLM data spans various periods from 1994 to 2019 and was allocated to the 47 deltas by Nienhuis and van de Wal (2021). The assumption was applied to those areas with the unavailability of the data within 1 degree, the values of VLM are zero.

Nienhuis and van de Wal (2021) constrained the VLM rates to a range of -10 mm to 10 mm, with negative values denoting uplifting. Furthermore, Nienhuis and van de Wal (2021) assumed that the VLM will remain the same for future conditions. Therefore, in this research, the value of the VLM over the years is constant.

To conclude, the composite effect of Relative Sea-Level Rise (RSLR) in this study encompasses both sea-level rise and Vertical Land Movement (VLM). In the context of this research, the positive values in VLM indicate a downward trend in land elevation. Consequently, for RSLR, the dynamics entail an upward trend, given that the VLM exacerbates the impact of sea-level rise. Conversely, negative values in VLM signify landward aggradation, mitigating the impact of sea-level rise on delta areas.

2.2.3 Fluvial Sediment Supply

The fluvial sediment supply (Q_{river}) utilized in this research is retrieved from the projection performed by Dunn (2019) specifically for the 47 major deltas. The projection employed the hydrogeomorphic model of WBMsed (Cohen et al., 2013, 2014) under 12 distinct environmental change scenarios, encapsulating the influences of climate change, socio-economic development, and dam construction throughout the 21st century. The model conducted by Dunn (2019) executed daily time steps, but for the purposes of this research, mean annual sediment fluxes were extracted for analysis.

The 12 scenarios considered in this study were derived from a combination of the Representative Concentration Pathway (RCP), including RCP 2.6, 4.5, 6.0, and 8.5 (Jones et al., 2011); three Shared Socio-economic Pathway (SSP) denoted as SSP 1, 2, and 3 (Murakami and Yamagata, 2019); and a projection of future dam construction (Lehner et al., 2011a; b; Zarfl et al., 2015). However, the RCP 6.0 scenarios were not utilized in this study due to the unavailability of specific data on RSLR scenarios. Therefore, the finalized scenarios were reduced to 9, as illustrated in Figure 2.3, following the formulation undertaken by Dunn (2019). In addition to the 9 scenarios, the dataset also encompasses the isolated impacts of each component, including three RCPs (RCP

2.6, 4.5, and 8.5), three SSPs (SSP 1, 2, and 3), and dam construction. This comprehensive dataset allows for a nuanced exploration of the distinct influences exerted by each factor on the projected outcomes.

Shared Socioeconomic Pathway	Representative Concentration Pathway: RCP 2.6	RCP 4.5	RCP 8.5
SSP 1	Low Climate Change Low Socioeconomic Challenge	Moderate Climate Change Low Socioeconomic Challenge	High Climate Change Low Socioeconomic Challenge
SSP 2	Low Climate Change Moderate Socioeconomic Challenge	Moderate Climate Change Moderate Socioeconomic Challenge	High Climate Change Moderate Socioeconomic Challenge
SSP 3	Low Climate Change High Socioeconomic Challenge	Moderate Climate Change High Socioeconomic Challenge	High Climate Change High Socioeconomic Challenge

Figure 2.3 The construction of the 9 scenarios of the future river sediment supply.

2.3 Model Scenario Definition

The model conducted in this research is expressed by Equation 5, wherein the sea-level data and fluvial sediment flux (Q_{river}) components are characterized by a variety scenario, each corresponding to different of climatic, socio-economics, and future dam construction as detailed in 2.2.2 and 2.2.3. Therefore, new scenarios are made to accommodate the variety of scenarios within each component.

On one hand, the sea-level data incorporates three climate-change scenarios: RCP 2.6, 4.5, and 8.5. On the other hand, the fluvial sediment supply integrates twelve scenarios combining climate-change scenarios of RCP 2.6, 4.5, 6.0, and 8.5 with Socio-economic scenarios of SSP 1, 2, and 3, including the future dam scenarios within each scenario. Notably, RCP 6.0 is excluded from the sea-level data, thus this research omits the corresponding scenario from the sediment supply components, resulting in a total of nine scenarios. This approach ensures alignment and consistency in the analysis of both sea-level and fluvial sediment flux components. To understand the combination of the scenarios, the explanation can be seen in Figure 2.3.

The sea-level and sediment supply data utilized in this study are based on the projection within the 21st century. Each dataset is structured with an annual time step, and adjustments have been made to align with data availability. Consequently, the datasets cover the period from 2007 to 2100, reflecting the timeframe of the projections and ensuring consistency in the analysis over this specified temporal range.

2.4 Test Against Observations

The model's validation process involves a comparison against the observed delta area change from 1985-2015, utilizing the average of two global land-water change models (Donchyts et al., 2016; Pekel et al., 2016). These models, based on Landsat 30 m imagery (NASA, 2024), was used as a benchmark for validating the model's prediction. The validation outcomes are quantified by the Rooted Mean Squared Error (RMSE) of 5.73 km² and the Coefficient of Determination (R^2) of 2.44. Figure 2.4 visually represents the comparison, demonstrating a distribution that closely aligns with the indicator line, indicating a reasonable degree of correspondence between model predictions and observed data. A fraction of the fluvial sediment (f_r) equal to 0.9 in the model to enhance the accuracy of the projection. The specific value is selected based on its optimization, resulting in the best value for the RMSE and R^2. By using f_r = 0.9, the model aims to achieve a more favorable alignment with observed data, providing improved performance in terms of both accuracy and predictive capability.

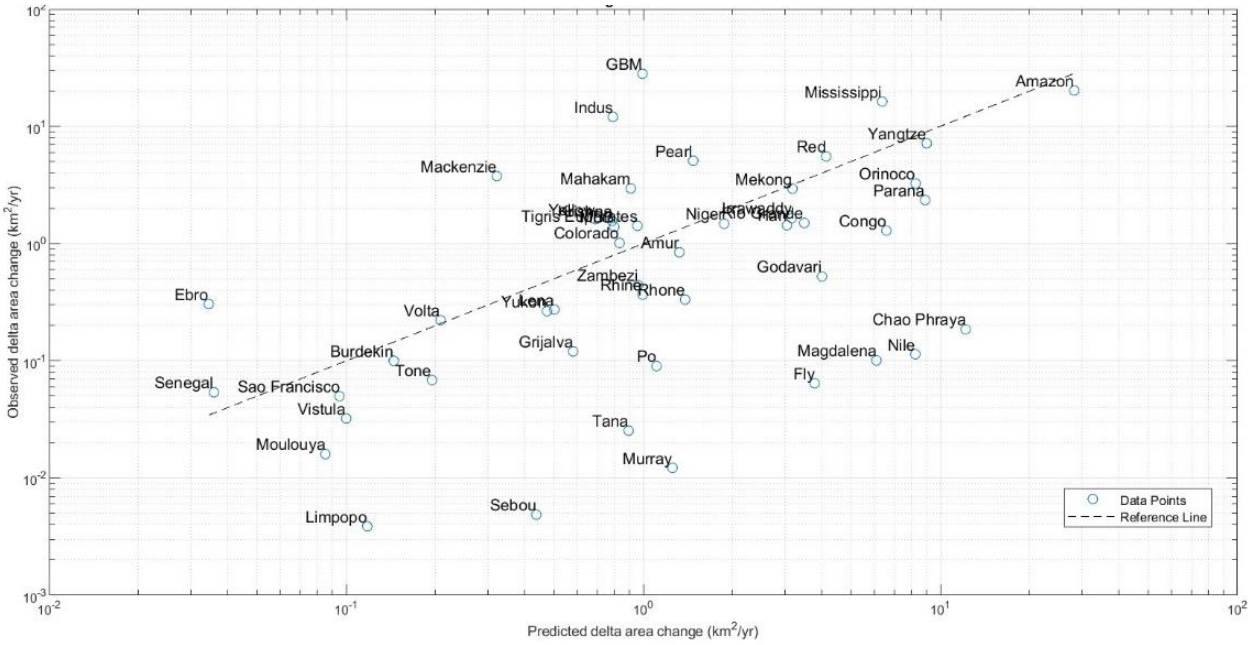

Figure 2.4 Predicted versus observed delta area change 1985 – 2015 for individual deltas

3 Results

3.1 Future Delta Area Changes

3.1.1 Global Projection of Future Major Delta

Figure 3.1 visually depicts the evolution of A_{delta} over the years from 2007 to 2100, showcasing delta area loss for all scenarios. The result of the future delta area projections reveals that the total A_{delta} for 47 major deltas by the end of the 21st century falls within the range of 634,119.82 to 647,356.43 km^2 across all nine scenarios. The value suggests that under each scenario, the 47 major deltas are anticipated to undergo a reduction in area, with the projected losses ranging 4,924.57 km^2 to 18,161.18 km^2. In percentage terms, this equates to a potential loss of 0.75 to 2.78% of their total area by the year 2100. The variability in this projection indicates the sensitivity of delta areas to different scenarios considered in this study.

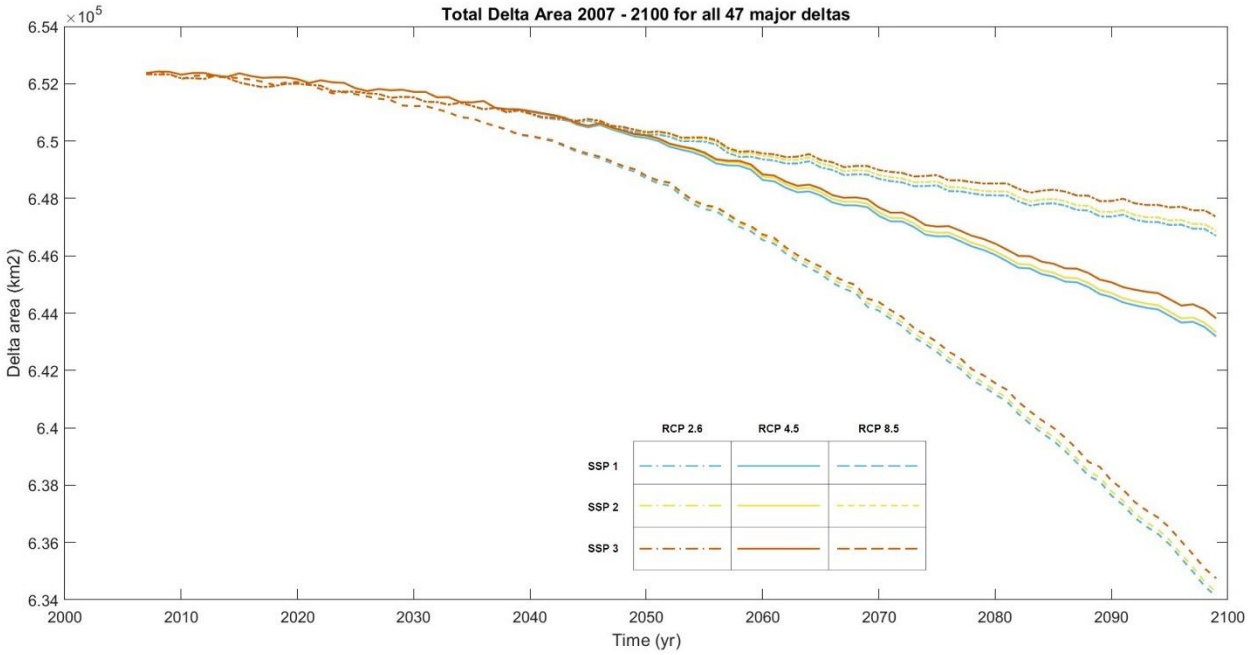

Figure 3.1 Total delta area for 47 major deltas from 2007 to 2100 across RCP and SSP scenarios.

To understand the differences among scenarios, the model results for the total of 47 major deltas are summarized in Table 3-1. The scenario aligned with the highest socio-economic challenges (SSP 3) and the smallest climate change (RCP 2.6) generates the lowest area changes compared to the other scenarios, resulting in a total area loss of 4,924.57 km^2. On the other hand, the scenario entailing the lowest socio-economic challenges (SSP 1) and the largest climate change (RCP 8.5) exhibits the highest area loss, accounting for 18,161.18 km^2. The contrast between the scenarios is significant, with the latter being almost five times in magnitude compared to the former scenario of SSP 3, RCP 2.6.

Despite the notable difference between the scenarios featuring the largest and the smallest area loss, certain patterns emerge. Scenarios characterized by minimal climate change (RCP 2.6) exhibit a relatively consistent range of area changes. Similarly, scenarios associated with moderate climate change (RCP 4.5) and the largest climate change (RCP 8.5) manifest similar patterns. However, the RCP 8.5 scenarios yield the highest delta area loss (with a mean delta area loss of 2.74% across three same climate scenarios) by 2100, followed by RCP 4.5 scenarios (with a mean delta area loss of 1.35% across three same climate scenarios) and RCP 2.6 scenarios (with a mean delta area loss of 0.81% across three same climate scenarios).

Likewise, within the same climate change frameworks, the three socio-economic scenarios display observable differences, even though with relatively modest compared to the variations among climate change scenarios. Notably, the SSP 3 scenarios demonstrate the least pronounced area change, followed by SSP 2 and SSP 1, respectively. The observed in delta area changes under all scenarios suggest indicating a correlation with the climate-change and socio-economic settings of each scenario.

Table 3-1 Total A_{delta}, area change, and percentage change for all 47 major deltas at the end of the 21st century. Negative values indicate the loss of the area.

Scenario	A_{delta} in km2	Area Change	percentage change
SSP 1 RCP 2.6	646,693.14	-5,587.86	-0.86%
SSP 1 RCP 4.5	643,184.87	-9,096.13	-1.39%
SSP 1 RCP 8.5	634,119.82	-18,161.18	-2.78%
SSP 2 RCP 2.6	646,859.08	-5,421.92	-0.83%
SSP 2 RCP 4.5	643,334.08	-8,946.92	-1.37%
SSP 2 RCP 8.5	634,272.35	-18,008.65	-2.76%
SSP 3 RCP 2.6	647,356.43	-4,924.57	-0.75%
SSP 3 RCP 4.5	643,814.89	-8,466.11	-1.30%
SSP 3 RCP 8.5	634,752.76	-17,528.24	-2.69%

3.1.2 Local Projection for Future Delta Area

The individual delta projections provide insights into how changes occur in each delta. Figure 3.2 presents the changes in the delta area for each of the 47 major deltas by the year 2100 across all scenarios. The projection maps show that a majority of the 47 major deltas are expected to undergo a reduction in delta area by 2100. However, noteworthy exceptions are observed in South America, where several deltas, including the Amazon, Magdalena, Orinoco, and Parana, are projected to experience a relatively significant increase in delta area.

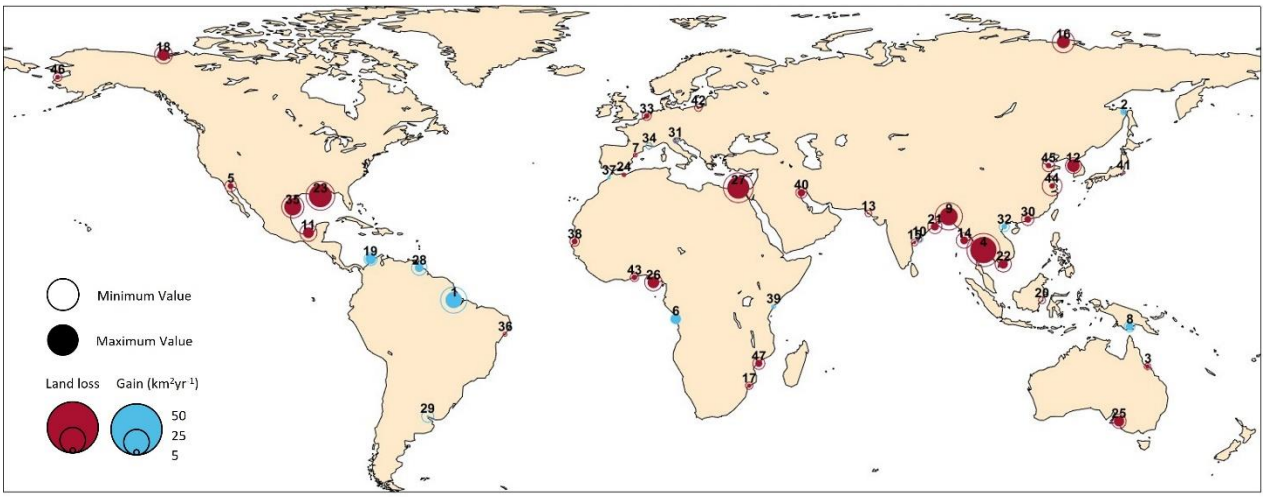

Figure 3.2 Projection of delta area change by 2100 across RCP and SSP scenarios. Each dot represents minimum and maximum rate of changes (km2/yr). 1 Amazon, 2 Amur, 3 Burdekin, 4 Chao Phraya, 5 Colorado, 6 Congo, 7 Ebro, 8 Fly, 9 GBM, 10 Godavari, 11 Grijalva, 12 Han, 13 Indus, 14 Irrawaddy, 15 Krishna, 16 Lena, 17 Limpopo, 18 Mackenzie, 19 Magdalena, 20 Mahakam, 21 MBB,22 Mekong, 23 Mississippi, 24 Moulouya, 25 Murray, 26 Niger, 27 Nile, 28 Orinoco, 29 Paraná, 30 Pearl, 31 Po, 32 Red, 33 Rhine, 34 Rhône, 35 Rio Grande, 36 São Francisco, 37 Sebou, 38 Senegal, 39 Tana, 40 Tigris Euphrates, 41 Tone, 42 Vistula, 43 Volta, 44 Yangtze, 45 Yellow, 46 Yukon, 47 Zambezi

Figure 3.3a visually presents the contributions of individual deltas to the overall area changes by the year 2100. The changes vary from a reduction of 2,536 km^2 for the Chao Phraya to an increase of 1,603 km^2 for the Amazon. Importantly, specific deltas exhibit substantial changes, significantly influencing the total delta area changes, with dA_{delta} exceeding 1,000 km2 for each delta. These prominent deltas include the Amazon, Chao Phraya, GBM, Mississippi, and Nile Delta. It is noteworthy that these specific deltas are among the 10 largest deltas (refer to 2.1.1).

To contextualize the impact of dA_{delta} on each delta, Figure 3.3b demonstrates the percentage change in dA_{delta} compared to the initial A_{delta} at the beginning of the century. The percent dA_{delta} ranges from a reduction of 22.81% for the Han to an increase of 10.09% for the Congo. Moreover, the Han and Murray exhibit the highest area loss relative to their initial A_{delta}, with the latter showing up to 22,75% area loss. In contrast, Magdalena and Congo will experience considerably significant area gains by 8.68% and 10.09%, respectively. Despite exhibiting the largest area gain, the Amazon's dA_{delta} contributes relatively small changes, accounting for up to 1.47% of its initial A_{delta}. Conversely, the Chao Phraya, the delta with the largest area loss, has its projected dA_{delta} contributing up to 10.70% loss, making it the third largest loss contribution out of 47 major deltas.

Equally important, consistent patterns emerge for each delta, with some deltas consistently experiencing a gain in area changes. For instance, among 47 major deltas, 10 deltas are anticipated to consistently gain area for all nine scenarios by the year of 2100. These deltas

include the Amazon, Amur, Congo, Fly, Magdalena, Orinoco, Parana, Red, Sebou, and Tana. On the other hand, 33 deltas are expected to undergo area loss by 2100. Additionally, the four remaining deltas exhibit fluctuating changes for certain scenarios by 2100. These four deltas include Godavari, Po, Rhône, and Tone.

Table 3-2 provides a detailed overview of the delta area changes for the four deltas under consideration across nine scenarios. While these deltas do not exhibit a collective pattern, specific trends can be observed from each delta individually. Taking Godavari as an example, under most scenarios, the delta area tends to gain, with the exception of SSP 1, RCP 8.5 scenario and SSP 2, RCP 8.5 scenario. Interestingly, when comparing these scenarios with others that share the same RCP 8.5, such as SSP 3, RCP 8.5 scenario, a trend emerges suggesting that higher SSP values lead to a tendency for delta area gain. This phenomenon appears to influence the remaining deltas as well, indicating the interplay between climate change and socio-economic settings, where the impacts of fluvial sediment supply and RSLR compensate for each other.

Despite some major deltas experiencing area gain by 2100, the findings reveal that all 47 major deltas will encounter a decrease in the changes of delta area rate by 2100. Figure 3.3c visually represents the changes in dA_{delta}/dt (km^2/yr) from 2007 – 2026 to 2081 – 2100 across nine scenarios, illustrating a universal decline in dA_{delta}/dt for all 47 major deltas by 2100. Notably, the Amazon, GBM, and Chao Phraya deltas exhibit the highest decrease, with reductions of up to 25.4 km^2/yr, 24.2 km^2/yr, 23.8 km^2/yr respectively. This outcome suggests that RSLR is likely to overcompensate for fluvial sediment supply by the end of the century, resulting in a decreasing trend indA_{delta}/dt.

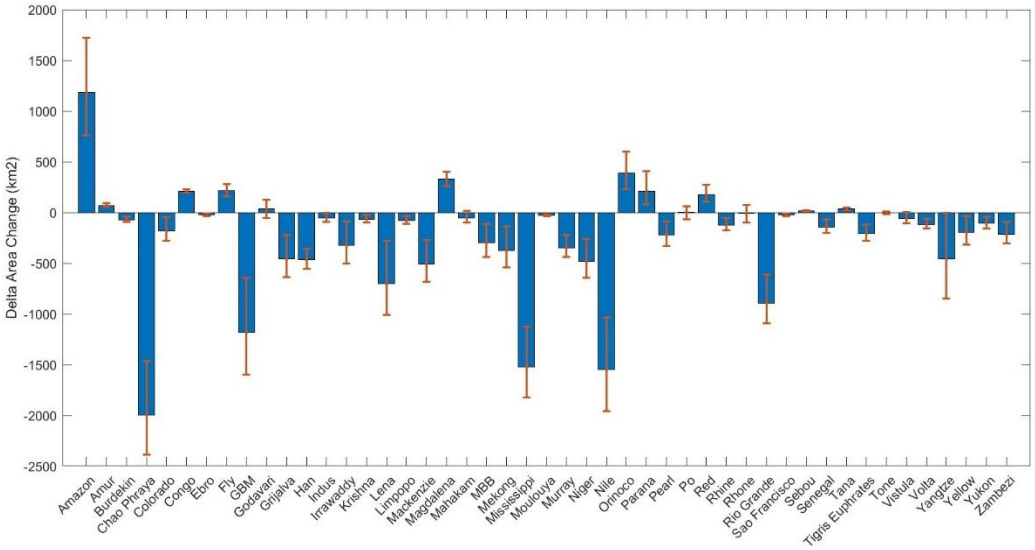

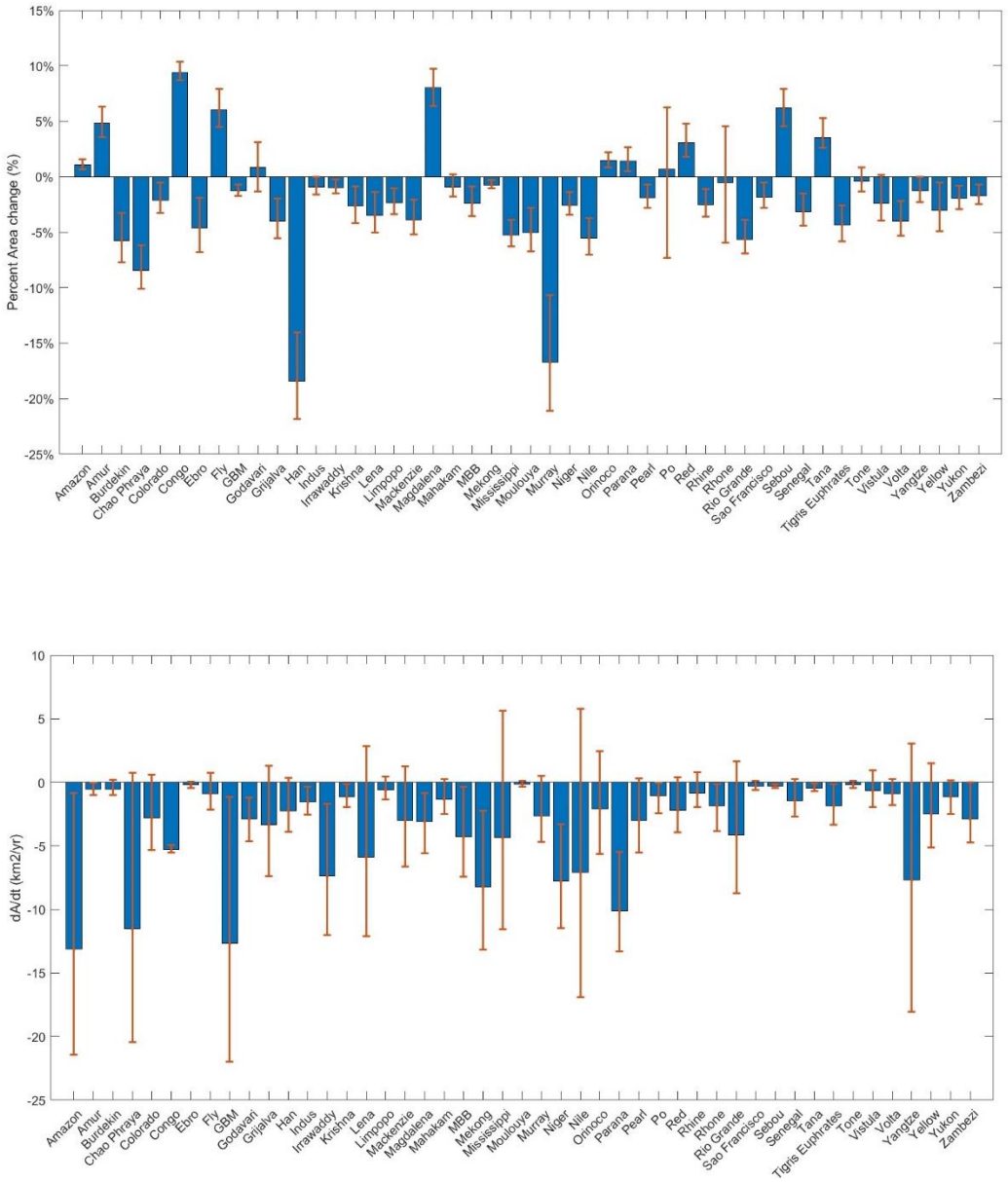

Figure 3.3 (a) projected individual mean delta area changes across nine scenarios for 47 major deltas, (b) percent individual area change compared to initial delta area, (c) Change in mean annual dA_{delta} (2007 – 2026 to 2081 – 2099). The bars represent the mean scenarios whereas the error bars represent the maximum and minimum result from the scenario ensemble for each delta.

Table 3-2 Deltas undergo different area changes by 2100 depending on the scenarios

	Scenario								
Delta Name	SSP 1 RCP 2.6	SSP 1 RCP 4.5	SSP 1 RCP 8.5	SSP 2 RCP 2.6	SSP 2 RCP 4.5	SSP 2 RCP 8.5	SSP 3 RCP 2.6	SSP 3 RCP 4.5	SSP 3 RCP 8.5

Godavari	51.04	21.56	-56.98	67.50	38.04	-40.27	120.51	90.80	13.00
Po	-3.71	-16.80	-46.72	-1.29	-14.39	-44.33	81.87	66.03	36.83
Rhône	5.89	-27.77	-93.59	20.49	-13.47	-79.24	83.25	46.78	-19.13
Tone	4.39	-0.27	-17.67	4.39	-0.27	-17.67	4.39	-0.27	-17.67

3.2 Standalone Effect of Sediment Supply and RSLR Effects in Delta Dynamics

The impact of sediment supply and relative sea-level rise (RSLR) individually is examined by isolating each component within zero-value scenario, followed by comparing dA_{delta}/dt (km^2/yr) from 2007 – 2026 to 2081 – 2100 for each component effect. To illustrate, the assessment of how sediment supply influences delta area changes involve utilizing the zero value of sea-level for each delta. Subsequently, this value is combined with local vertical land movement (VLM) to establish the RSLR value. Similarly, to investigate the effect of RSLR, the zero value of sediment supply scenarios is employed. This approach allows for the systematic study of each component's influence on delta area changes, discerning which component has a greater impact on each delta and the overall delta system.

3.2.1 Global Standalone Effect to the 47 Major Deltas

The evaluation involves comparing each component to the projection results to quantify the extent of changes induced by the standalone effects of sediment supply or RSLR. Moreover, this analysis enables an investigation into the significance of changes in dA_{delta}/dt in the end of the century compared to the beginning of the century.

Figure 3.4 illustrates the percentage of the dA_{delta}/dt changes by the end of the century. The sediment effect shows relatively stagnant results across all SSP and RCP scenarios, ranging from approximately 25% to 30% of decline. On the other hand, the RSLR effect exhibits more significant changes across RCP scenarios, with ~1%, ~60%, and ~195% for RCP 2.6, RCP 4.5, and RCP 8.5, respectively. Furthermore, in addition to the significant changes across RCP scenarios, the RSLR effect also has higher percentage changes for RCP 4.5 and RCP 8.5 compared to the changes from sediment effect.

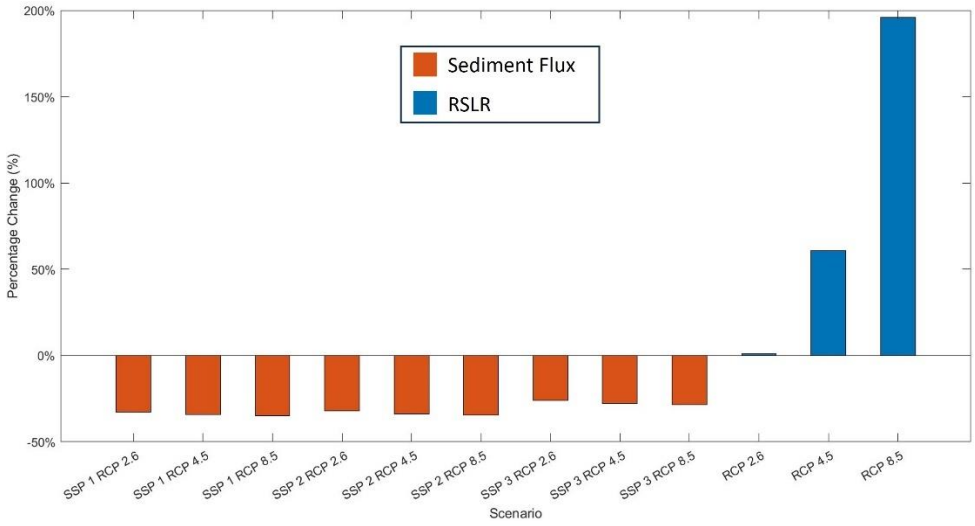

Figure 3.4 The percentage of changes in dA_{delta}/dt from 2007 – 2026 to 2081 – 2100 in fluvial sediment supply and RSLR for all 47 major deltas across SSP and RCP.

3.2.2 Standalone Effects on the Individual Deltas

The determination of which component overestimates the other can be ascertained through a comparison of the standalone changes effects driven the individual deltas. Figure 3.5 illustrates the relative sediment flux and RSLR changes between 2007 – 2026 and 2081 – 2100 for moderate scenario. Out of the 47 deltas, the RSLR changes effect compensates for the sediment supply effects in 40 deltas, while the remaining 7 deltas are primarily driven by sediment supply changes effects. Notable differences are observed in specific deltas. For instance, in deltas like Amazon, Chao Phraya, GBM, Mississippi, and Nile, the differences exceed 1000 km².

Notable deltas experiencing RSLR changes exceeding 100% include the Colorado, Parana, and Tone. Conversely, the sediment flux changes has the highest impact on the Indus and Congo deltas, with declines of 80% and 90%, respectively. Moreover, the decline in sediment flux changes is more pronounced. Specifically, out of the 7 deltas affected by sediment flux changes, 6 will experience a decline in sediment flux changes.

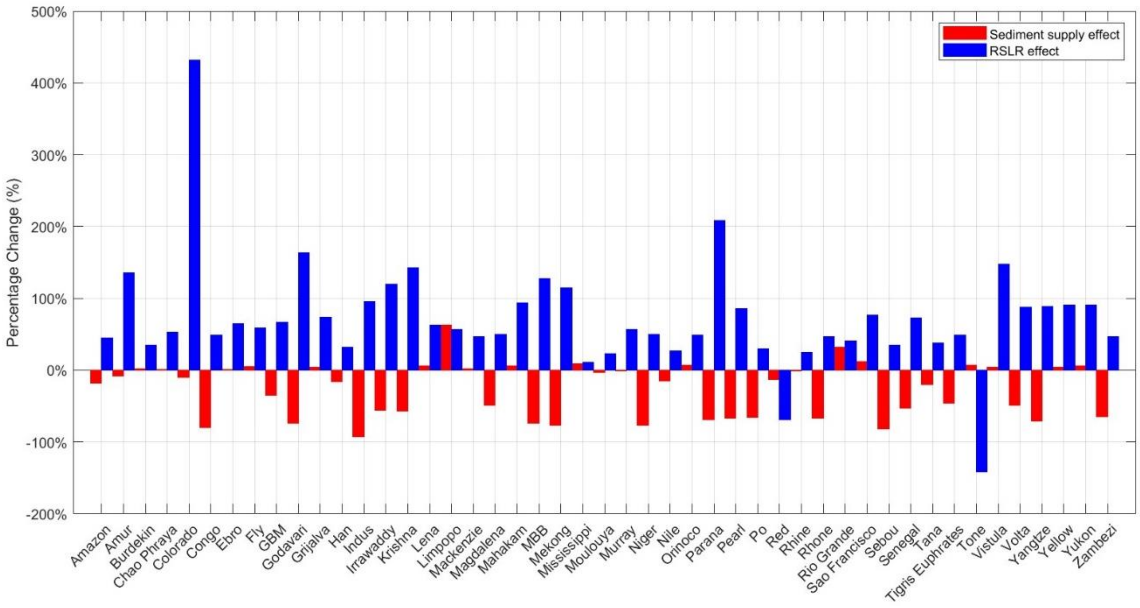

Figure 3.5 Relative sediment flux and RSLR change between 2007 - 2026 and 2081 – 2100 (moderate scenario) for individual deltas

3.3 RSLR and Sediment Flux Threshold

By employing Equation 5 with dA_{delta}/dt = 0, it is possible to determine the safety rate for both RSLR and sediment supply. This rate serves as a threshold to identify the maximum value of the RSLR rate that global, or individual deltas can withstand. Similarly, the threshold also establishes the minimum value required to maintain a sufficient sediment supply rate essential for the well-being of global and individual deltas. Using that assumption, thus following equating can be utilized for determining the threshold for the RSLR rate and sediment flux rate.

$$RSLR = \frac{Q_{river} \cdot f_r}{A_{delta}}$$

Equation 6

$$Q_{river} = \frac{RSLR \cdot A_{delta}}{f_r}$$

Equation 7

3.3.1 Threshold for the Global 47 Major Delta

By applying Equation 6 and setting the value for the global sediment supply, the threshold graph is depicted in Figure 3.6. For instance, following the moderate scenario (RCP 4.5 and SSP 2) for the 21st century, delta areas will initially experience a relatively safe situation, with the RSLR at 3.59 mm/yr and the threshold at 5.4 mm/yr. However, by the middle of the 21st century, the threshold decreases to 4.4 mm/yr, while the RSLR increases to 5.7 mm/yr, indicating that the RSLR will exceed the threshold. Similarly, by the end of the century, the threshold further decreases to 3.6 mm/yr, while the RSLR continues to rise to 6.28 mm/yr.

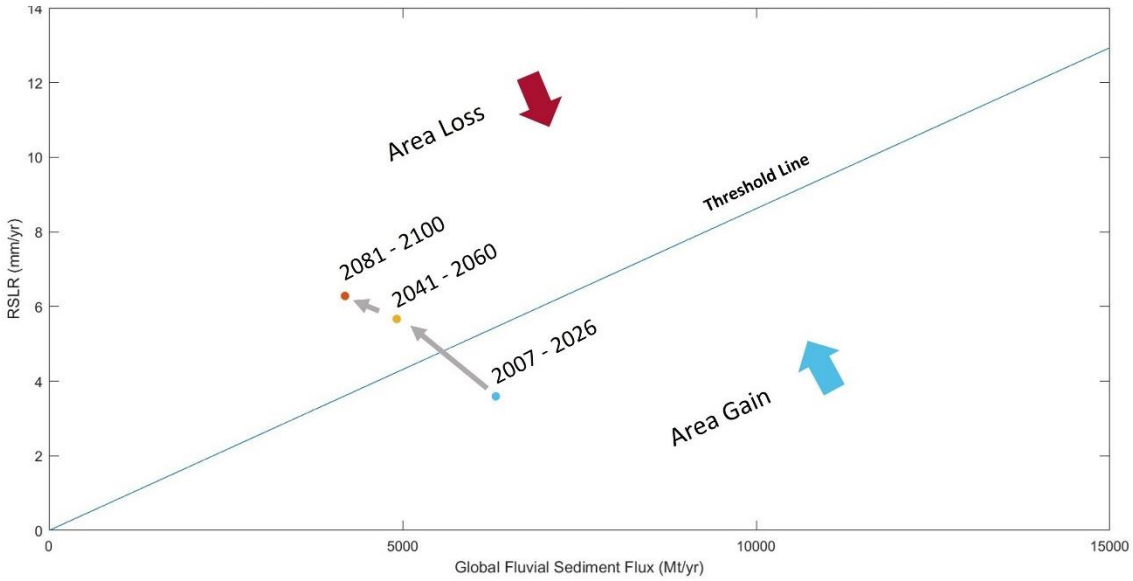

Figure 3.6 Global threshold of RSLR and sediment flux for 47 major deltas under the moderate scenario in the 21st century.

Establishing the sediment supply for the moderate scenario over the years, Figure 3.7 illustrates the threshold values for RSLR rate. The RSLR threshold decreases from 5.6 mm/yr to 3.6 mm/yr under the moderate sediment supply scenario, indicating that the global major delta should not exceed a rate of 3.6 mm/yr by the end of the year 2100. Furthermore, based on the time series graph, the threshold will be exceeded starting from 2039.

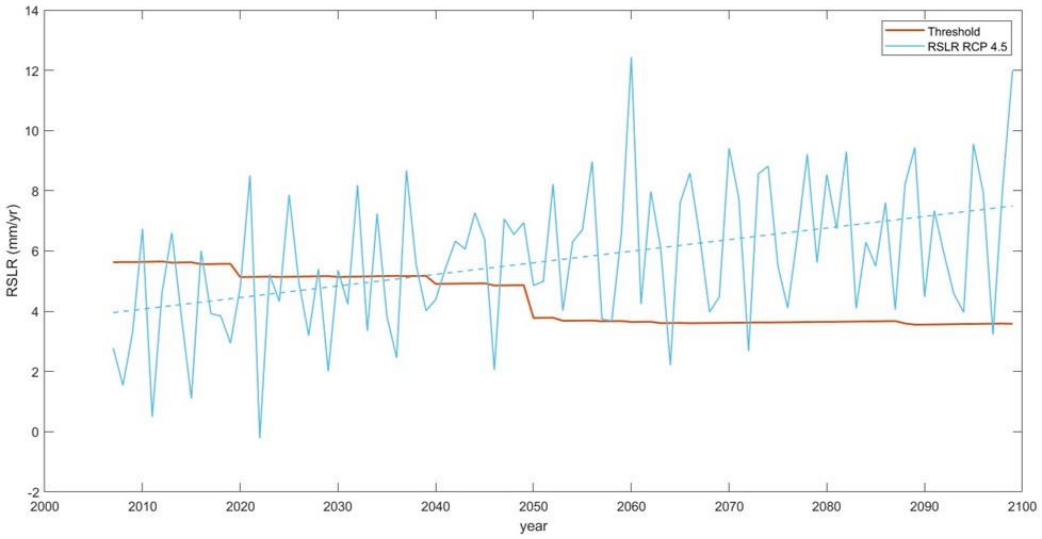

Figure 3.7 RSLR Threshold and RSLR time-series 2007 – 2100 under the moderate scenario.

3.3.2 Threshold for the Individual Deltas

Analyzing the threshold for individual deltas, assuming that deltas experience a moderate scenario for the RSLR rate and sediment supply rate, the thresholds will be illustrated as shown in Figure 3.8. The graph demonstrates the threshold for the last 10 years of the computation. Several key observations from Figure 3.8 include the deltas whose area is projected to decrease by 2100 (see Figure 3.3) showing low RSLR thresholds and higher sediment supply thresholds. For instance, GBM exhibits a low RSLR threshold, approximately 2 mm/yr and a significantly higher require sediment supply, around 1500 Mt/yr. Other than that, there is a notable delta with a relatively higher RSLR and higher sediment supply, but the delta seems to experience area gain by 2100. This occurrence could potentially be attributed to the high amount of sediment supply in the delta.

Furthermore, notably, some large deltas such as GBM, Mekong, Irrawaddy, and Yangtze, four out of the five largest deltas in this dataset (see Table 2-1), have low RSLR thresholds, indicating relative vulnerability to the threat of sea-level rise. On the contrary, smaller deltas with smaller A_{delta}, such as such as Ebro, Moulouya, and Sebou exhibit significantly higher RSLR thresholds. As expected from Equation 6 and Equation 7, A_{delta} appears to have a significant impact on the threshold of each individual delta, resulting in smaller A_{delta} will obtain higher RSLR threshold and lower sediment supply threshold. Consequently, deltas with smaller A_{delta} appears to be more resilient to the threat of sea-level rise and are better positioned to meet sufficient sediment flux requirements.

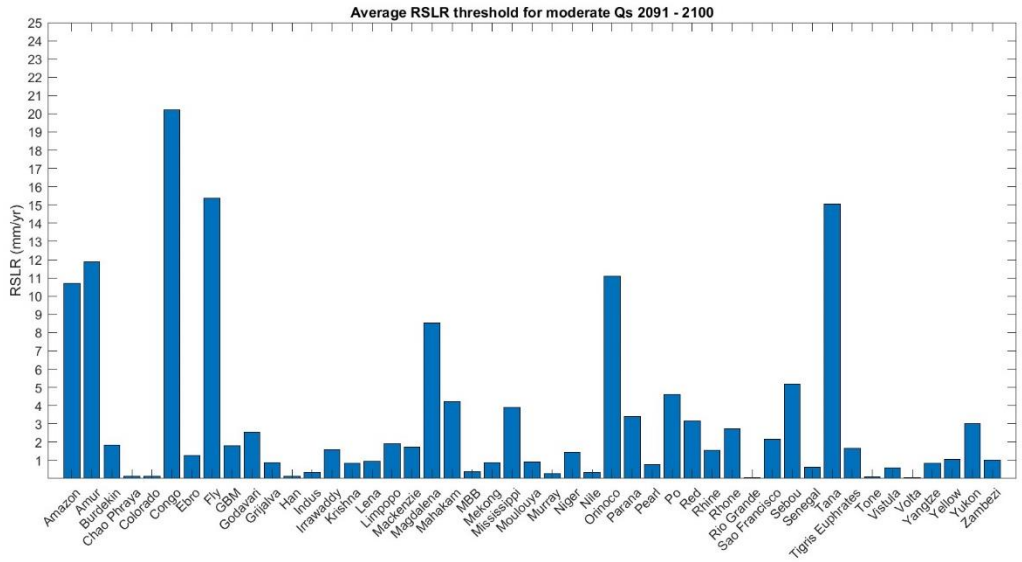

(a)

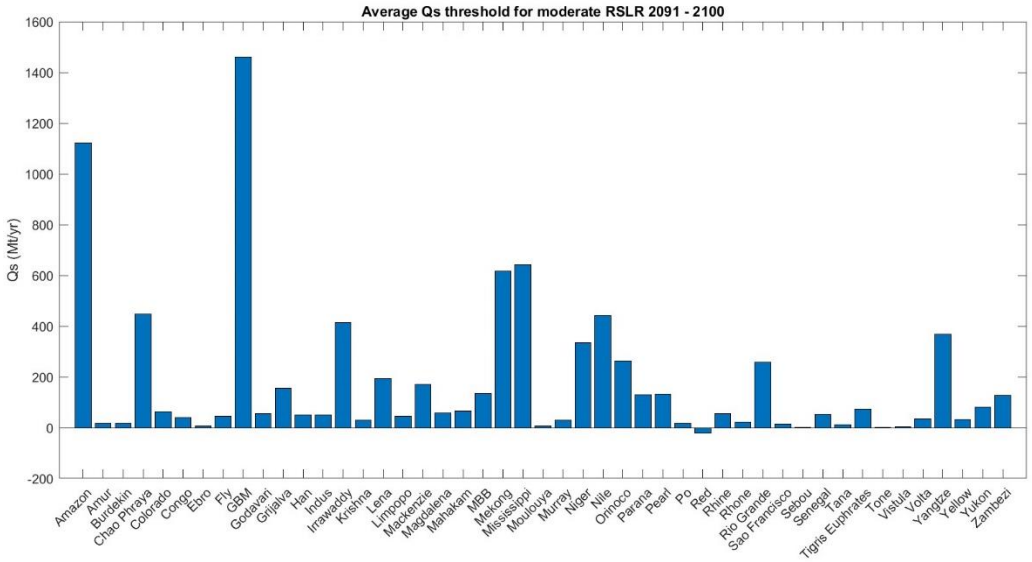

(b)

Figure 3.8 Average 10-year threshold for individual delta 2091 – 2100, (a) RSLR threshold, (b) sediment supply threshold

3.4 Driver Analysis

The sediment supply dataset from Dunn et al. (2019) offers a separate projection for each driver. Consequently, projections can be made for each driver to analyze their respective contributions

to delta area change. Three RCP scenarios, three SSP scenarios, and one dam construction scenario are estimated with the combination of the RCP input for the RSLR components.

Figure 3.9 illustrates the driver contributions for each individual delta under the moderate condition of sea-level rise input. The contribution of each delta is subsequently estimated, revealing that the majority of deltas are predominantly influenced by the effect of the SSP, with 28 deltas being most affected, followed by Dams with 14 deltas, and RCP predominantly affecting 5 deltas. Therefore, the anthropogenic changes (human activities and the dam construction) here play the main role in driving the sediment flux effect on delta area changes.

Some notable results can be observed, such as the Amazon experiencing the highest dam effect, followed by the Parana. Besides, the GBM and will have the highest SSP effect along with the dam construction. An interesting outcome is the Chao Phraya that will have similar results for the RCP, SSP, and the dam construction.

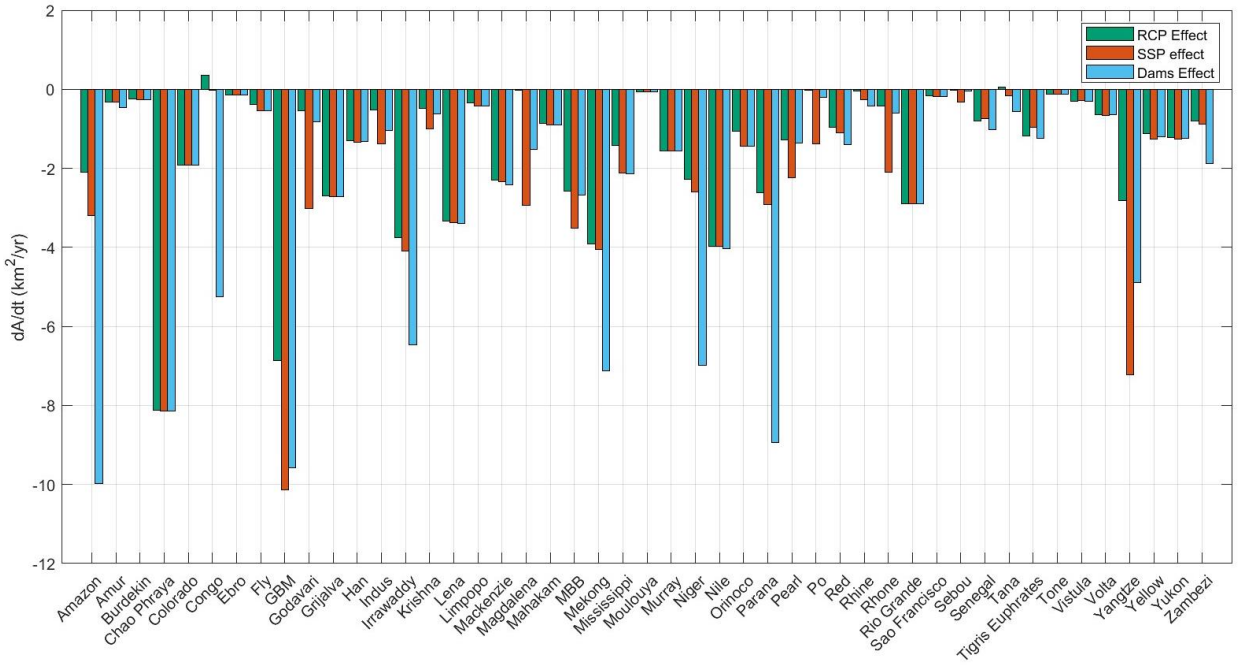

Figure 3.9 Relative delta area change rate between 2007 – 2026 and 2081 – 2100 for different sediment flux drivers under moderate scenario of RSLR

4 Discussion

4.1 Synthesis Main Finding

4.1.1 The Influence of Climate Pathways and Socio-Economic Pathway

The findings presented in 3.1.1 reveal distinct patterns of impact associated with each climate pathway and socio-economic pathway on the projected future delta. The analysis indicates that scenarios characterized by the highest socio-economic challenges (SSP 3) and the smallest climate change (RCP 2.6) tend to exhibit the smallest area changes. Conversely, scenarios featuring the lowest socio-economic challenges (SSP 1) and the largest (RCP 8.5) are associated with the largest area changes.

The influence of climate change appears to exert a more significant impact on delta areas compared to socio-economic challenges, as depicted in Figure 3.1. The observed patterns in changes induced by socio-economic challenges suggest that increased anthropogenic influence results in higher sediment flux, attributable to reduced economic development and less effective land management practices (Dunn et al., 2019). On the other hand, the effects of climate change indicate that higher RCP values lead to larger dA_{delta} losses, attributed to the higher RSLR as a result of higher carbon emission (Oppenheimer et al., 2019).

Across all scenarios, a consistent pattern emerges for the majority of deltas, with 10 deltas experiencing area gain and 33 deltas undergoing area loss. This uniformity suggests a predominant factor influencing whether certain deltas gain or lose area. However, four specific deltas–the Godavari, Po, Rhône, and Tone–exhibit fluctuating projections across the nine scenarios outlined in Table 3-2.

Despite the variations in projected gains or losses, the influence of socio-economic and climate change factors remains consistent. Specifically, higher SSP values result in larger dA_{delta}, while larger RCP indicates larger dA_{delta} loss. This finding underscores the intricate interplay between climate change and socio-economic settings, where the impacts of fluvial sediment supply and RSLR compensate for each other.

4.1.2 The Standalone Effect and the Sediment Delivery Driver Effect to the Projection

The evaluation of standalone effects aims to identify which component, either anthropogenic and climate change combined fluvial sediment supply or climate change RSLR, exhibit a more significant impact on the future delta area. The changes of each component in the end of century are compared to the beginning of the century to see which one has more effect than the other. Globally, for all 47 major deltas, the climate change RSLR overwhelms the effects of anthropogenic and climate change combined fluvial sediment supply by two times for average dA_{delta} across scenarios for each component (Figure 3.4). In Dunn (2019), the larger RCP resulted in smallest decrease in fluvial sediment supply, supporting the dA_{delta} gain. However, in this research, this effect seems to be overcompensated by the overwhelming RSLR effect. As a result, the larger RCP here appears to have the larger dA_{delta} loss.

The alteration in deltaic land area is likely to be influenced predominantly by local variability (Tessler et al., 2018). Therefore, conducting an individualized analysis for each delta is imperative to comprehend how each specific delta responds to the effects of RSLR and fluvial sediment supply. Despite the pronounced impact of RSLR on all 47 major deltas, a subset of 12 deltas is projected to undergo an increase in delta area (refer Table 4-1), driven more significantly by the influence of fluvial sediment delivery. Among these, seven deltas exhibit a substantial change, experiencing an area gain exceeding 100 km^2. Notably, six of these deltas with significant area gain are situated in South America, Africa, and Oceania, where there is an observed rise in sediment flux attributed to land-use changes (Dethier et al., 2022). Furthermore, the deltas of Amazon, Magdalena, Orinoco, and Fly stand out due to their limited upstream dam infrastructure, allowing them to continue receiving a substantial portion of sediment fluxes (Tessler et al., 2018).

In contrast to the observed gain in A_{delta} in the projected future delta. The dA_{delta}/dt is anticipated to decrease for all deltas from the period 2007 – 2026 to 2081 – 2100. This trend holds true even for the deltas that are gaining area by 2100 (refer Table 4-1). This phenomenon is attributed to the continual rise in RSLR, while the fluvial sediment supply is expected to decrease after a certain point, primarily influenced by anthropogenic factors such as changing land management practices and dam construction. Consequently, the gradual dominance of the RSLR effect is anticipated to prevail for all 47 major deltas over time.

Table 4-1 Deltas with gaining area

Delta Name	Location	Mean dA_{delta} (km^2)	Mean Rate change (km^2/yr)
Amazon	South America	1179.88	-13.13
Amur	Asia	69.89	-0.57
Congo	Africa	208.52	-5.27
Fly	Oceania	212.71	-0.91
Godavari	Asia	33.91	-2.89
Magdalena	South America	331.55	-3.09
Orinoco	South America	388.80	-2.09
Parana	South America	211.18	-10.13
Po	Europe	6.39	-1.07
Red	Asia	174.96	-2.20
Sebou	Africa	15.23	-0.28
Tana	Africa	32.51	-0.46

Furthermore, the decline in the rate of change for all deltas can be attributed to the impact of dam construction on the projection of fluvial sediment delivery. In the model, the construction timeline was set until 2050, and thereafter, the reservoir capacity remained unchanged. Figure 3.9 illustrates how certain deltas will undergo significant reductions in dA_{delta}/dt influenced by the dam construction. Notably, the Amazon will experience the most substantial decrease in

dA_{delta}/dt, even though it contributes to the largest gain compared to other deltas. The majority of anthropogenic changes are expected to be the primary factor influencing how sediment supply affects delta area in the future.

4.1.3 Delta Area and the Threshold

The individual threshold of each delta shows some patterns to the delta that consider larger and smaller. Some large deltas such as GBM, Mekong, Irrawaddy, and Yangtze, four out of the five largest deltas in this dataset, have low RSLR thresholds, indicating relative vulnerability to the threat of sea-level rise. On the contrary, smaller deltas with smaller A_{delta}, such as such as Ebro, Moulouya, and Sebou exhibit significantly higher RSLR thresholds. As expected from Equation 6 and Equation 7, A_{delta} appears to have a significant impact on the threshold of each individual delta, resulting in smaller A_{delta} will obtain higher RSLR threshold and lower sediment supply threshold. Consequently, deltas with smaller A_{delta} appears to be more resilient to the threat of seal-level rise and area better positioned to meet sufficient sediment flux requirements.

Furthermore, the results indicate that deltas projected to experience area loss by 2100 tend to have a lower RSLR threshold and a higher sediment flux threshold. This phenomenon arises from the model's projection of RSLR and fluvial sediment delivery, aligning the thresholds with the anticipated changes in delta area. However, the Amazon presents an intriguing finding. Despite having the second-highest fluvial sediment delivery threshold, the Amazon is projected to gain area by 2100. This can be attributed to the high sediment flux, which is expected to remain relatively safe by 2100, thereby sustaining the delta area change.

4.2 Limitations and Future Work

This research builds upon the work of Nienhuis and van de Wal (2021) by incorporating the fluvial sediment delivery projection provided by Dunn (2019). Prior to the inclusion of sediment supply projections, the data remained constant over the years. The introduction of sediment supply projections enhances our understanding of the rate changes occurring in each delta over time. However, it's important to note that the delta subsidence rate in this research remains constant since the beginning of the century. In reality, subsidence rates are likely to change over the years due to human activities, particularly in large deltas (Biljsma et al., 1995; Erban et al., 2014). The incorporation of subsidence rate variability would contribute to an improved representation of the relative sea-level rise (RSLR) outcomes. Additionally, the uncertainties also arise when the estimation of the subsidence rate over time, sea-level change, and present-day morphology are conducted, thus limit the prediction accuracy (Nienhuis and van de Wal, 2021).

The sediment supply projection in this research assumes that dam construction occurs by 2050. However, it is important to note that the effects of dams are unlikely to remain constant after 2050. The uncertain factors include the timeline, location, and specifications of the dams, making predictions regarding dam construction challenging.

This research model assumes that the morphodynamic can be expressed as the morpho-kinematic mass balance approach, which typically holds over long period of time (Nienhuis and van de Wal, 2021). On the other hand, the model also assumes a linear delta response to RSLR and fluvial sediment flux, which covers relatively short period compared to the age of the delta. Therefore, these assumptions introduce uncertainties in spatiotemporal investigations.

5 Conclusion

This research investigates the response of the river delta to future RSLR and future fluvial sediment flux. The study focuses on 47 major deltas, chosen to represent a diverse range of climates, geomorphologies, population densities, and socio-economic conditions. The primary objectives are to project changes in the area of these major deltas and identify the principal factors driving these changes. Consequently, the key findings of this study are as follows:

- Total 47 major deltas are projected to experience land loss, ranging from approximately 5,000 km2 to 18,000 km2, representing a potential loss of 0.75% to 2.78% of their total area by the year 2100. Among these, 35 deltas are expected to undergo land loss, with the Han and Murray deltas projected to lose approximately 23% of their area by 2100. Conversely, the remaining 12 deltas are anticipated to undergo area gain, with the Magdalena and Congo deltas exhibiting the highest area gain compared to their initial delta area, with increases of 8.5% and 10%, respectively. However, despite these gains, the delta area change rate is expected to decline for all 47 major deltas by the end of the century compared to the beginning, indicating the possibility of area loss for deltas that experienced gains in the 21st century, in the subsequent century.
- The comparison between the fluvial sediment flux and RSLR components reveals the predominant driver of change for the 47 major deltas. Notably, the study finds that the relative RSLR change between 2007 – 2026 and 2081 - 2100 exhibits more profound effects, showing significant variations across RCP scenarios. Specifically, the RSLR change is estimated at approximately 1%, 60%, and 195% for RCP 2.6, RCP 4.5, and RCP 8.5, respectively. Conversely, the relative sediment flux remains relatively stagnant across all SSP and RCP scenarios, showing declines ranging from approximately 25% to 30%. Regarding the contributions of sediment flux to delta area change, anthropogenic influences, including human activities and dam construction, emerge as the primary drivers of change by 2100, affecting 32 deltas compared to climate change, which affects 5 deltas. Moreover, the projected thresholds for the 47 major deltas are expected to be exceeded by 2039, with a rate of 5.1 mm/yr, declining gradually to 3.6 mm/yr over the years. Conversely, RSLR is anticipated to rise, exacerbating the threat of area change across the deltas.

The research findings indicate that the 47 major deltas are likely to experience area loss by 2100, with projections conducted for each delta providing insights into their respective responses and the primary drivers of change. These outcomes offer valuable information for developing strategies to address the challenges faced by each delta. However, it's essential to consider the uncertainties inherent in the research, which necessitate ongoing development of the model and refinement of the results. This underscores the need for continued research and adaptation in planning and management efforts aimed at mitigating the impacts on delta ecosystems and communities.

References

Anderson, T.R., C.H. Fletcher, M.M. Barbee, B.M. Romine, S. Lemmo, et al. 2018. Modeling multiple sea level rise stresses reveals up to twice the land at risk compared to strictly passive flooding methods. Sci Rep 8(1). doi: 10.1038/s41598-018-32658-x.

Anderson, W., J. Lorenzo-Trueba, and V. Voller. 2019. A geomorphic enthalpy method: Description and application to the evolution of fluvial-deltas under sea-level cycles. Comput Geosci 130: 1–10. doi: 10.1016/j.cageo.2019.05.006.

Biljsma, L., C.N. Ehler, R.J.T. Klein, S.M. Kulshrestha, R. Mclean, et al. 1995. Coastal zones and small islands.

Blewitt, G., W. Hammond, and C. Kreemer. 2018. Harnessing the GPS Data Explosion for Interdisciplinary Science. doi: https://doi. org/10.1029/2018EO104623.

Blum, M.D., and T.E. Törnqvist. 2000. Fluvial responses to climate and sea-level change: A review and look forward. Sedimentology 47(SUPPL. 1): 2–48. doi: 10.1046/j.1365-3091.2000.00008.x.

Cohen, S., A.J. Kettner, and J.P.M. Syvitski. 2014. Global suspended sediment and water discharge dynamics between 1960 and 2010: Continental trends and intra-basin sensitivity. Glob Planet Change 115: 44–58. doi: 10.1016/j.gloplacha.2014.01.011.

Cohen, S., A.J. Kettner, J.P.M. Syvitski, and B.M. Fekete. 2013. WBMsed, a distributed global-scale riverine sediment flux model: Model description and validation. Comput Geosci 53: 80–93. doi: 10.1016/j.cageo.2011.08.011.

Dethier, E.N., C.E. Renshaw, and F.J. Magilligan. 2022. Rapid changes to global river suspended sediment flux by humans.

Donchyts, G., F. Baart, H. Winsemius, N. Gorelick, J. Kwadijk, et al. 2016. Earth's surface water change over the past 30 years. Nat Clim Chang 6(9): 810–813. doi: 10.1038/nclimate3111.

Dunn, F.E., S.E. Darby, R.J. Nicholls, S. Cohen, C. Zarfl, et al. 2019. Projections of declining fluvial sediment delivery to major deltas worldwide in response to climate change and anthropogenic stress. Environmental Research Letters 14(8). doi: 10.1088/1748-9326/ab304e.

Edmonds, D.A., R.L. Caldwell, E.S. Brondizio, and S.M.O. Siani. 2020. Coastal flooding will disproportionately impact people on river deltas. Nat Commun 11(1). doi: 10.1038/s41467-020-18531-4.

Erban, L.E., S.M. Gorelick, and H.A. Zebker. 2014. Groundwater extraction, land subsidence, and sea-level rise in the Mekong Delta, Vietnam. Environmental Research Letters 9(8). doi: 10.1088/1748-9326/9/8/084010.

Ericson, J.P., C.J. Vörösmarty, S.L. Dingman, L.G. Ward, and M. Meybeck. 2006. Effective sea-level rise and deltas: Causes of change and human dimension implications. Glob Planet Change 50(1–2): 63–82. doi: 10.1016/j.gloplacha.2005.07.004.

Fagherazzi, S., and I. Overeem. 2007. Models of deltaic and inner continental shelf landform evolution. Annu Rev Earth Planet Sci 35: 685–715. doi: 10.1146/annurev.earth.35.031306.140128.

Giosan, L., J. Syvitski, S. Constantinescu, and J. Day. 2014. Climate change: protect the world deltas. Nature: 31–33. doi: https://doi.org/10.1038/516031a.

Gregory, J.M., S.M. Griffies, C.W. Hughes, J.A. Lowe, J.A. Church, et al. 2019. Concepts and Terminology for Sea Level: Mean, Variability and Change, Both Local and Global. Surv Geophys 40(6): 1251–1289. doi: 10.1007/s10712-019-09525-z.

Hamlington, B.D., A.S. Gardner, E. Ivins, J.T.M. Lenaerts, J.T. Reager, et al. 2020. Understanding of Contemporary Regional Sea-Level Change and the Implications for the Future. Reviews of Geophysics 58(3). doi: 10.1029/2019RG000672.

Helland-Hansen, W., and O.J. Martinsen. 1966. Shoreline trajectories and sequences: description of variable depositional-dip scenarios. Journal of Sedimentary Research 66(4): 670–688. doi: https://doi.org/10.1306/D42683DD-2B26-11D7-8648000102C1865D.

Higgins, S.A. 2016. Review: Advances in delta-subsidence research using satellite methods. Hydrogeol J 24(3): 587–600. doi: 10.1007/s10040-015-1330-6.

Hinkel, J., D. Lincke, A.T. Vafeidis, M. Perrette, R.J. Nicholls, et al. 2014. Coastal flood damage and adaptation costs under 21st century sea-level rise. Proc Natl Acad Sci U S A 111(9): 3292–3297. doi: 10.1073/pnas.1222469111.

Hoogendoorn, R.M., I. Overeem, and J.E.A. Storms. 2008. Process-response modelling of fluvio-deltaic stratigraphy. Comput Geosci 34(10): 1394–1416. doi: 10.1016/j.cageo.2008.02.006.

Ibáñez, C., J.W. Day, and E. Reyes. 2014. The response of deltas to sea-level rise: Natural mechanisms and management options to adapt to high-end scenarios. Ecol Eng 65: 122–130. doi: 10.1016/j.ecoleng.2013.08.002.

Jones, C.D., J.K. Hughes, N. Bellouin, S.C. Hardiman, G.S. Jones, et al. 2011. The HadGEM2-ES implementation of CMIP5 centennial simulations. Geosci Model Dev 4(3): 543–570. doi: 10.5194/gmd-4-543-2011.

Juhász, L., J. Xu, and R.W. Parkinson. 2023. Beyond the Tide: A Comprehensive Guide to Sea-Level-Rise Inundation Mapping Using FOSS4G. Geomatics 3(4): 522–540. doi: 10.3390/geomatics3040028.

Kim, W., A. Dai, T. Muto, and G. Parker. 2009. Delta progradation driven by an advancing sediment source: Coupled theory and experiment describing the evolution of elongated deltas. Water Resour Res 45(6). doi: 10.1029/2008WR007382.

Kim, W., C. Paola, V.R. Voller, and J.B. Swenson. 2006. Experimental measurement of the relative importance of controls on shoreline migration. Journal of Sedimentary Research 76(2): 270–283. doi: 10.2110/jsr.2006.019.

Kirezci, E., I.R. Young, R. Ranasinghe, S. Muis, R.J. Nicholls, et al. 2020. Projections of global-scale extreme sea levels and resulting episodic coastal flooding over the 21st Century. Sci Rep 10(1). doi: 10.1038/s41598-020-67736-6.

Kopp, R.E., C.C. Hay, C.M. Little, and J.X. Mitrovica. 2015. Geographic Variability of Sea-Level Change. Curr Clim Change Rep 1(3): 192–204. doi: 10.1007/s40641-015-0015-5.

Kuchar, J., G. Milne, M. Wolstencroft, R. Love, L. Tarasov, et al. 2018. The Influence of Sediment Isostatic Adjustment on Sea Level Change and Land Motion Along the U.S. Gulf Coast. J Geophys Res Solid Earth 123(1): 780–796. doi: 10.1002/2017JB014695.

Lai, S.Y.J., and H. Capart. 2009. Reservoir infill by hyperpycnal deltas oyer bedrock. Geophys Res Lett 36(8). doi: 10.1029/2008GL037139.

Lehner, B., C.R. Liermann, C. Revenga, C. Vörömsmarty, B. Fekete, et al. 2011a. Global Reservoir and Dam Database. Version 1 (GRanDv1): Dams, Revision 01. Palisades, New York: NASA Socioeconomic Data and Applications Center (SEDAC). doi: https://doi.org/10.7927/H4N877QK.

Lehner, B., C.R. Liermann, C. Revenga, C. Vörömsmarty, B. Fekete, et al. 2011b. High-resolution mapping of the world's reservoirs and dams for sustainable river-flow management. Front Ecol Environ 9(9): 494–502. doi: 10.1890/100125.

Li, J., V. Ganti, C. Li, and H. Wei. 2022. Upstream migration of avulsion sites on lowland deltas with river-mouth retreat. Earth Planet Sci Lett 577. doi: 10.1016/j.epsl.2021.117270.

Mcmanus, J. 2002. Deltaic responses to changes in river regimes.

Murakami, D., and Y. Yamagata. 2019. Estimation of gridded population and GDP scenarios with spatially explicit statistical downscaling. Sustainability (Switzerland) 11(7). doi: 10.3390/su11072106.

Muto, T. 2001. SHORELINE AUTORETREAT SUBSTANTIATED IN FLUME EXPERIMENTS.

NASA. 2024. Landsat 4/5/7/8. https://www.usgs.gov/landsat-missions (accessed 12 January 2024).

Nicholls, R.J. 2011. Planning for the impacts of sea level rise. Oceanography 24(2): 144–157. doi: 10.5670/oceanog.2011.34.

Nicholls, R.J., and A. Cazenave. 2010. Sea-Level Rise and Its Impact on Coastal Zones.

Nienhuis, J.H., A.D. Ashton, D.A. Edmonds, A.J.F. Hoitink, A.J. Kettner, et al. 2020. Global-scale human impact on delta morphology has led to net land area gain. Nature 577(7791): 514–518. doi: 10.1038/s41586-019-1905-9.

Nienhuis, J.H., W. Kim, G.A. Milne, M. Quock, A.B.A. Slangen, et al. 2023. Annual Review of Earth and Planetary Sciences River Deltas and Sea-Level Rise. doi: 10.1146/annurev-earth-031621.

Nienhuis, J.H., T.E. Törnqvist, K.L. Jankowski, A.M. Fernandes, and M.E. Keogh. 2017. A new subsidence map for coastal Louisiana. GSA Today 27(9): 58–59. doi: 10.1130/GSATG337GW.1.

Nienhuis, J.H., and R.S.W. van de Wal. 2021. Projections of Global Delta Land Loss From Sea-Level Rise in the 21st Century. Geophys Res Lett 48(14). doi: 10.1029/2021GL093368.

Oppenheimer, M., B. Glavovic, J. Hinkel, R. van de Wal, A.K. Magnan, et al. 2019. Sea Level Rise and Implications for Low-Lying Islands, Coasts and Communities Supplementary Material In: IPCC Special Report on the Ocean and Cryosphere in a Changing Climate. Poh Poh Wong.

Pekel, J.F., A. Cottam, N. Gorelick, and A.S. Belward. 2016. High-resolution mapping of global surface water and its long-term changes. Nature 540(7633): 418–422. doi: 10.1038/nature20584.

Pfeffer, J., and P. Allemand. 2016. The key role of vertical land motions in coastal sea level variations: A global synthesis of multisatellite altimetry, tide gauge data and GPS measurements. Earth Planet Sci Lett 439: 39–47. doi: 10.1016/j.epsl.2016.01.027.

Shirzaei, M., J. Freymueller, T.E. Törnqvist, D.L. Galloway, T. Dura, et al. 2021. Measuring, modelling and projecting coastal land subsidence. Nat Rev Earth Environ 2(1): 40–58. doi: 10.1038/s43017-020-00115-x.

Swenson, J.B. 2005. Fluviodeltaic response to sea level perturbations: Amplitude and timing of shoreline translation and coastal onlap. J Geophys Res Earth Surf 110(3). doi: 10.1029/2004JF000208.

Syvitski, J.P.M. 2008. Deltas at risk. Sustainability Science. p. 23–32

Syvitski, J.P.M., and A. Kettner. 2011. Sediment flux and the anthropocene. Philosophical Transactions of the Royal Society A: Mathematical, Physical and Engineering Sciences 369(1938): 957–975. doi: 10.1098/rsta.2010.0329.

Syvitski, J.P.M., A.J. Kettner, I. Overeem, E.W.H. Hutton, M.T. Hannon, et al. 2009. Sinking deltas due to human activities. Nat Geosci 2(10): 681–686. doi: 10.1038/ngeo629.

Syvitski, J.P.M., C.J. Vörösmarty, A.J. Kettner, and P. Green. 2005. Impact of Humans on the Flux of Terrestrial Sediment to the Global Coastal Ocean.

Tessler, Z.D., C. Vörösmarty, M. Grossberg, I. Gladkova, H. Aizenman, et al. 2015. Profiling risk and sustainability in coastal deltas of the world. Science (1979) 349(6248): 638–643. doi: 10.1126/science.aab3574.

Tessler, Z.D., C.J. Vörösmarty, I. Overeem, and J.P.M. Syvitski. 2018. A model of water and sediment balance as determinants of relative sea level rise in contemporary and future deltas. Geomorphology 305: 209–220. doi: 10.1016/J.GEOMORPH.2017.09.040.

Tozer, B., D.T. Sandwell, W.H.F. Smith, C. Olson, J.R. Beale, et al. 2019. Global Bathymetry and Topography at 15 Arc Sec: SRTM15+. Earth and Space Science 6(10): 1847–1864. doi: 10.1029/2019EA000658.

Wolinsky, M.A. 2009. A unifying framework for shoreline migration: 1. Multiscale shoreline evolution on sedimentary coasts. J Geophys Res Earth Surf 114(1). doi: 10.1029/2007JF000855.

Wolstencroft, M., Z. Shen, T.E. Törnqvist, G.A. Milne, and M. Kulp. 2014. Understanding subsidence in the Mississippi Delta region due to sediment, ice, and ocean loading: Insights from geophysical modeling. J Geophys Res Solid Earth 119(4): 3838–3856. doi: 10.1002/2013JB010928.

Woodworth, P.L., A. Melet, M. Marcos, R.D. Ray, G. Wöppelmann, et al. 2019. Forcing Factors Affecting Sea Level Changes at the Coast. Surv Geophys 40(6): 1351–1397. doi: 10.1007/s10712-019-09531-1.

Yu, S.Y., T.E. Törnqvist, and P. Hu. 2012. Quantifying Holocene lithospheric subsidence rates underneath the Mississippi Delta. Earth Planet Sci Lett 331–332: 21–30. doi: 10.1016/j.epsl.2012.02.021.

Zarfl, C., A.E. Lumsdon, J. Berlekamp, L. Tydecks, and K. Tockner. 2015. A global boom in hydropower dam construction. Aquat Sci 77(1): 161–170. doi: 10.1007/s00027-014-0377-0.

6 Appendix

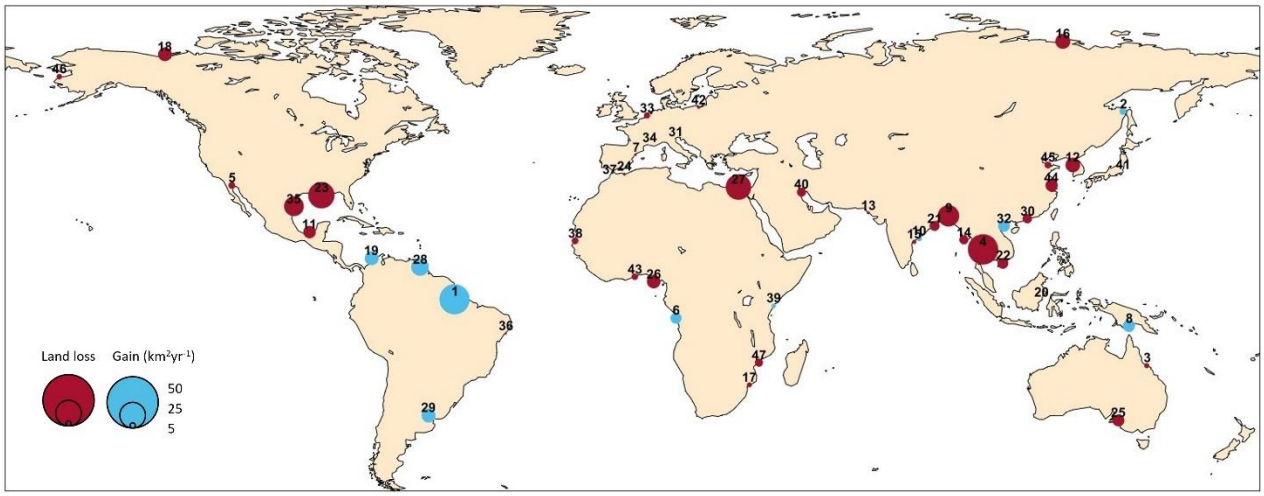

Figure 6.1 Projection of delta area change by 2100 for SSP 1 RCP 2.6 scenario. Each dot represents mean rate of changes (km2/yr). 1 Amazon, 2 Amur, 3 Burdekin, 4 Chao Phraya, 5 Colorado, 6 Congo, 7 Ebro, 8 Fly, 9 GBM, 10 Godavari, 11 Grijalva, 12 Han, 13 Indus, 14 Irrawaddy, 15 Krishna, 16 Lena, 17 Limpopo, 18 Mackenzie, 19 Magdalena, 20 Mahakam, 21 MBB,22 Mekong, 23 Mississippi, 24 Moulouya, 25 Murray, 26 Niger, 27 Nile, 28 Orinoco, 29 Paraná, 30 Pearl, 31 Po, 32 Red, 33 Rhine, 34 Rhône, 35 Rio Grande, 36 São Francisco, 37 Sebou, 38 Senegal, 39 Tana, 40 Tigris Euphrates, 41 Tone, 42 Vistula, 43 Volta, 44 Yangtze, 45 Yellow, 46 Yukon, 47 Zambezi

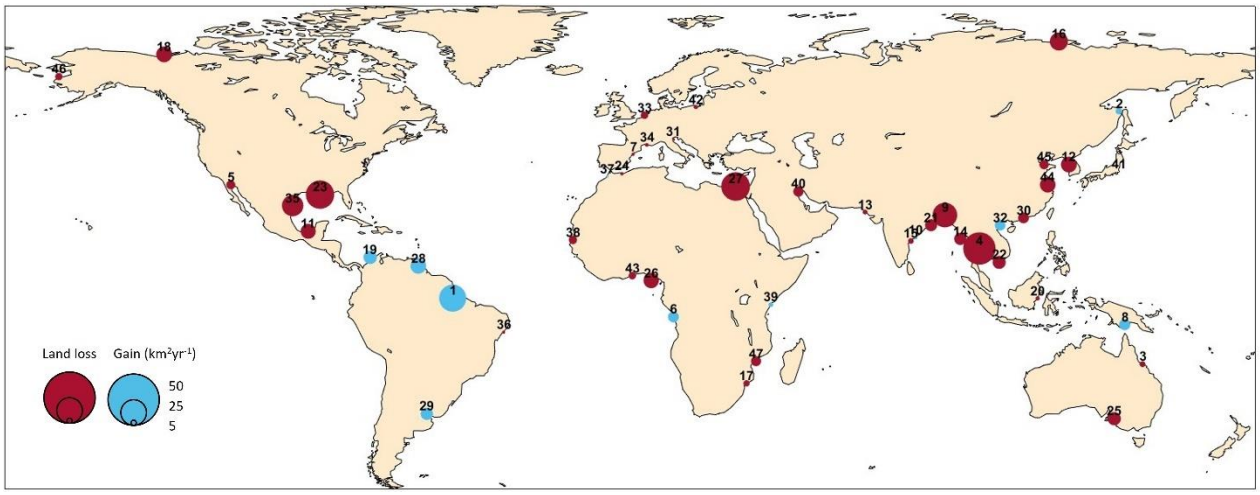

Figure 6.2 Projection of delta area change by 2100 for SSP 1 RCP 4.5 scenario. Each dot represents mean rate of changes (km2/yr). 1 Amazon, 2 Amur, 3 Burdekin, 4 Chao Phraya, 5 Colorado, 6 Congo, 7 Ebro, 8 Fly, 9 GBM, 10 Godavari, 11 Grijalva, 12 Han, 13 Indus, 14 Irrawaddy, 15 Krishna, 16 Lena, 17 Limpopo, 18 Mackenzie, 19 Magdalena, 20 Mahakam, 21 MBB,22 Mekong, 23 Mississippi, 24 Moulouya, 25 Murray, 26 Niger, 27 Nile, 28 Orinoco, 29 Paraná, 30 Pearl, 31 Po, 32 Red, 33 Rhine, 34 Rhône, 35 Rio

Grande, 36 São Francisco, 37 Sebou, 38 Senegal, 39 Tana, 40 Tigris Euphrates, 41 Tone, 42 Vistula, 43 Volta, 44 Yangtze, 45 Yellow, 46 Yukon, 47 Zambezi

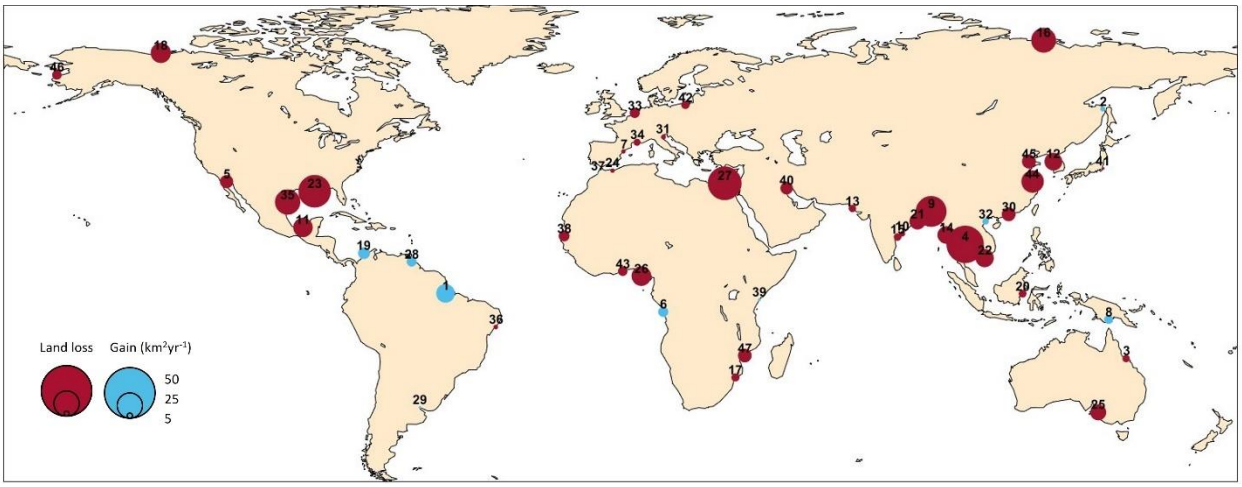

Figure 6.3 Projection of delta area change by 2100 for SSP 1 RCP 8.5 scenario. Each dot represents mean rate of changes (km2/yr). 1 Amazon, 2 Amur, 3 Burdekin, 4 Chao Phraya, 5 Colorado, 6 Congo, 7 Ebro, 8 Fly, 9 GBM, 10 Godavari, 11 Grijalva, 12 Han, 13 Indus, 14 Irrawaddy, 15 Krishna, 16 Lena, 17 Limpopo, 18 Mackenzie, 19 Magdalena, 20 Mahakam, 21 MBB,22 Mekong, 23 Mississippi, 24 Moulouya, 25 Murray, 26 Niger, 27 Nile, 28 Orinoco, 29 Paraná, 30 Pearl, 31 Po, 32 Red, 33 Rhine, 34 Rhône, 35 Rio Grande, 36 São Francisco, 37 Sebou, 38 Senegal, 39 Tana, 40 Tigris Euphrates, 41 Tone, 42 Vistula, 43 Volta, 44 Yangtze, 45 Yellow, 46 Yukon, 47 Zambezi

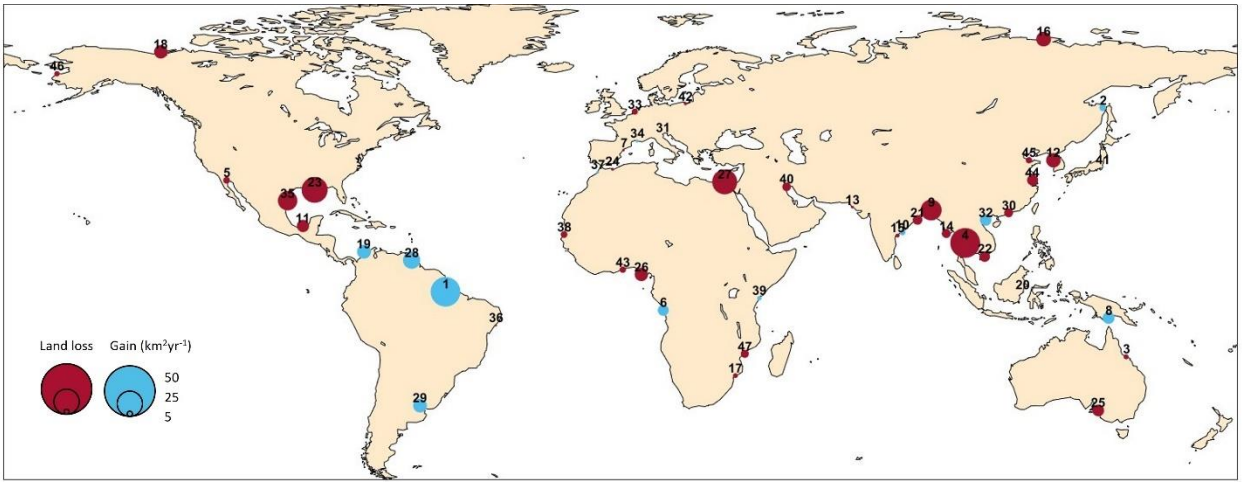

Figure 6.4 Projection of delta area change by 2100 for SSP 2 RCP 2.6 scenario. Each dot represents mean rate of changes (km2/yr). 1 Amazon, 2 Amur, 3 Burdekin, 4 Chao Phraya, 5 Colorado, 6 Congo, 7 Ebro, 8 Fly, 9 GBM, 10 Godavari, 11 Grijalva, 12 Han, 13 Indus, 14 Irrawaddy, 15 Krishna, 16 Lena, 17 Limpopo, 18 Mackenzie, 19 Magdalena, 20 Mahakam, 21 MBB,22 Mekong, 23 Mississippi, 24 Moulouya, 25

Murray, 26 Niger, 27 Nile, 28 Orinoco, 29 Paraná, 30 Pearl, 31 Po, 32 Red, 33 Rhine, 34 Rhône, 35 Rio Grande, 36 São Francisco, 37 Sebou, 38 Senegal, 39 Tana, 40 Tigris Euphrates, 41 Tone, 42 Vistula, 43 Volta, 44 Yangtze, 45 Yellow, 46 Yukon, 47 Zambezi

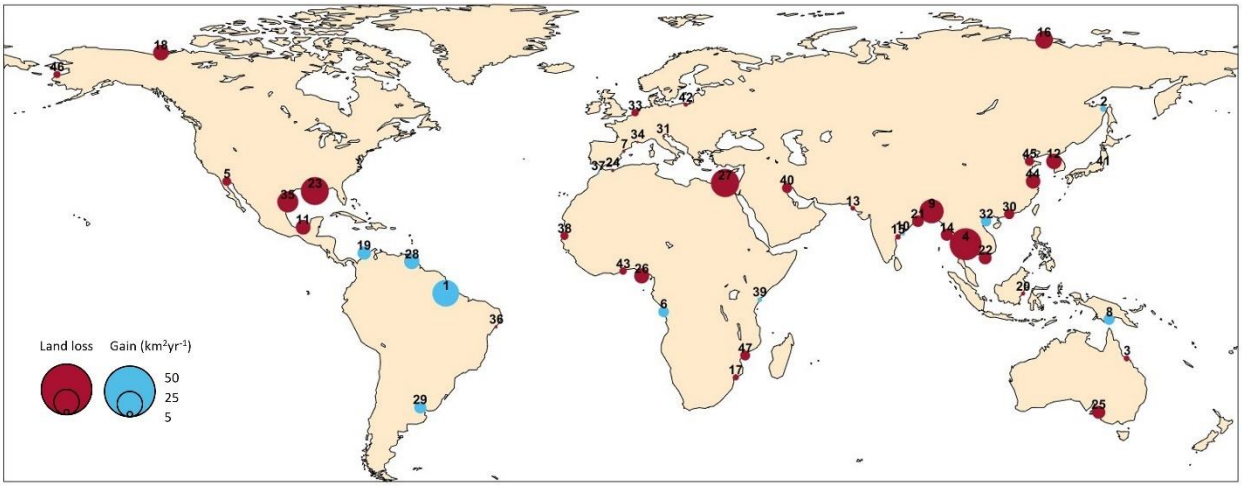

Figure 6.5 Projection of delta area change by 2100 for SSP 2 RCP 4.5 scenario. Each dot represents mean rate of changes (km2/yr). 1 Amazon, 2 Amur, 3 Burdekin, 4 Chao Phraya, 5 Colorado, 6 Congo, 7 Ebro, 8 Fly, 9 GBM, 10 Godavari, 11 Grijalva, 12 Han, 13 Indus, 14 Irrawaddy, 15 Krishna, 16 Lena, 17 Limpopo, 18 Mackenzie, 19 Magdalena, 20 Mahakam, 21 MBB,22 Mekong, 23 Mississippi, 24 Moulouya, 25 Murray, 26 Niger, 27 Nile, 28 Orinoco, 29 Paraná, 30 Pearl, 31 Po, 32 Red, 33 Rhine, 34 Rhône, 35 Rio Grande, 36 São Francisco, 37 Sebou, 38 Senegal, 39 Tana, 40 Tigris Euphrates, 41 Tone, 42 Vistula, 43 Volta, 44 Yangtze, 45 Yellow, 46 Yukon, 47 Zambezi

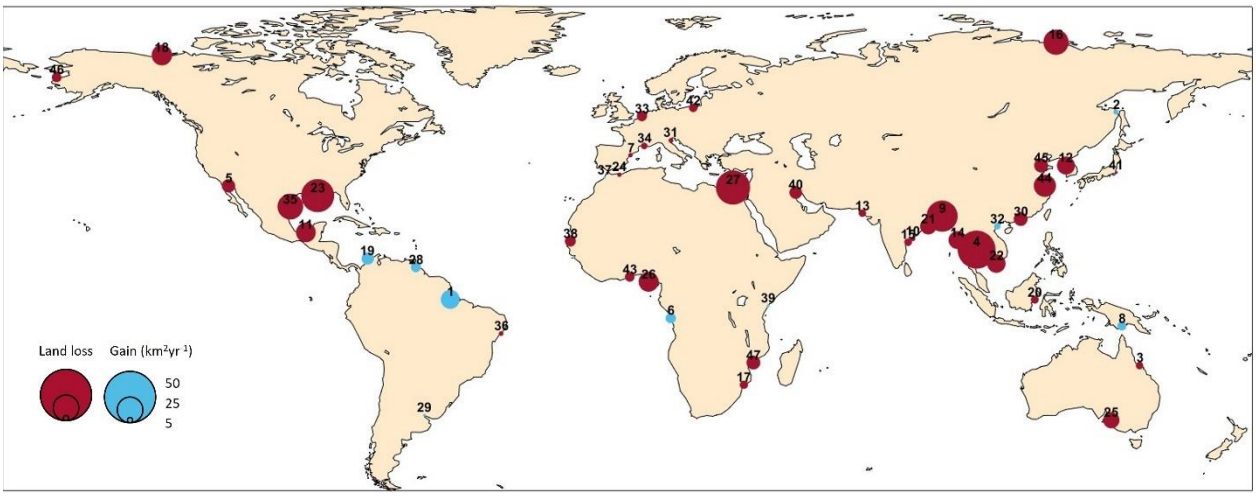

Figure 6.6 Projection of delta area change by 2100 for SSP 2 RCP 8.5 scenario. Each dot represents mean rate of changes (km2/yr). 1 Amazon, 2 Amur, 3 Burdekin, 4 Chao Phraya, 5 Colorado, 6 Congo, 7 Ebro, 8

Fly, 9 GBM, 10 Godavari, 11 Grijalva, 12 Han, 13 Indus, 14 Irrawaddy, 15 Krishna, 16 Lena, 17 Limpopo, 18 Mackenzie, 19 Magdalena, 20 Mahakam, 21 MBB,22 Mekong, 23 Mississippi, 24 Moulouya, 25 Murray, 26 Niger, 27 Nile, 28 Orinoco, 29 Paraná, 30 Pearl, 31 Po, 32 Red, 33 Rhine, 34 Rhône, 35 Rio Grande, 36 São Francisco, 37 Sebou, 38 Senegal, 39 Tana, 40 Tigris Euphrates, 41 Tone, 42 Vistula, 43 Volta, 44 Yangtze, 45 Yellow, 46 Yukon, 47 Zambezi

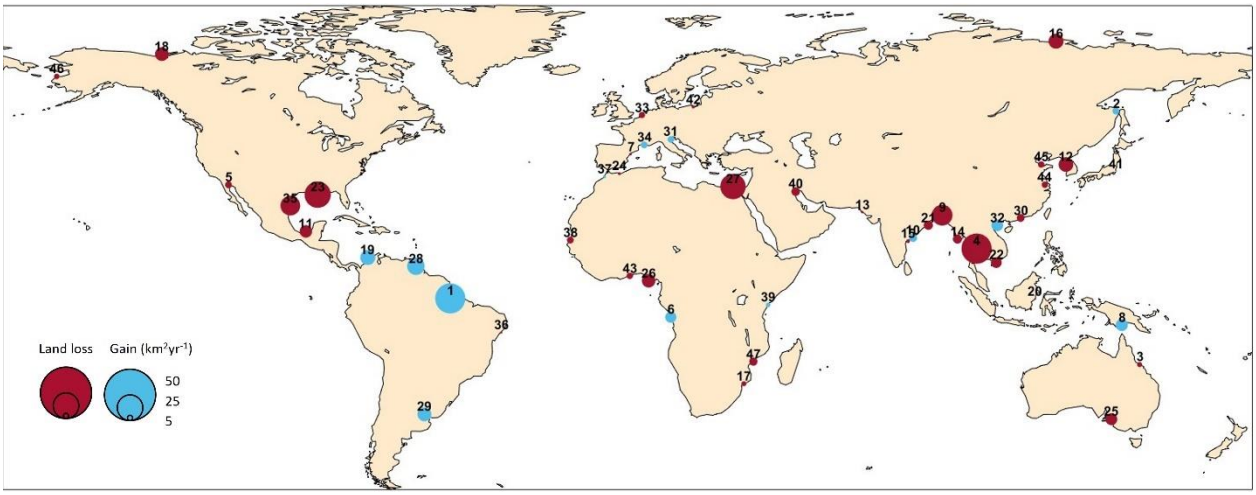

Figure 6.7 Projection of delta area change by 2100 for SSP 3 RCP 2.6 scenario. Each dot represents mean rate of changes (km2/yr). 1 Amazon, 2 Amur, 3 Burdekin, 4 Chao Phraya, 5 Colorado, 6 Congo, 7 Ebro, 8 Fly, 9 GBM, 10 Godavari, 11 Grijalva, 12 Han, 13 Indus, 14 Irrawaddy, 15 Krishna, 16 Lena, 17 Limpopo, 18 Mackenzie, 19 Magdalena, 20 Mahakam, 21 MBB,22 Mekong, 23 Mississippi, 24 Moulouya, 25 Murray, 26 Niger, 27 Nile, 28 Orinoco, 29 Paraná, 30 Pearl, 31 Po, 32 Red, 33 Rhine, 34 Rhône, 35 Rio Grande, 36 São Francisco, 37 Sebou, 38 Senegal, 39 Tana, 40 Tigris Euphrates, 41 Tone, 42 Vistula, 43 Volta, 44 Yangtze, 45 Yellow, 46 Yukon, 47 Zambezi

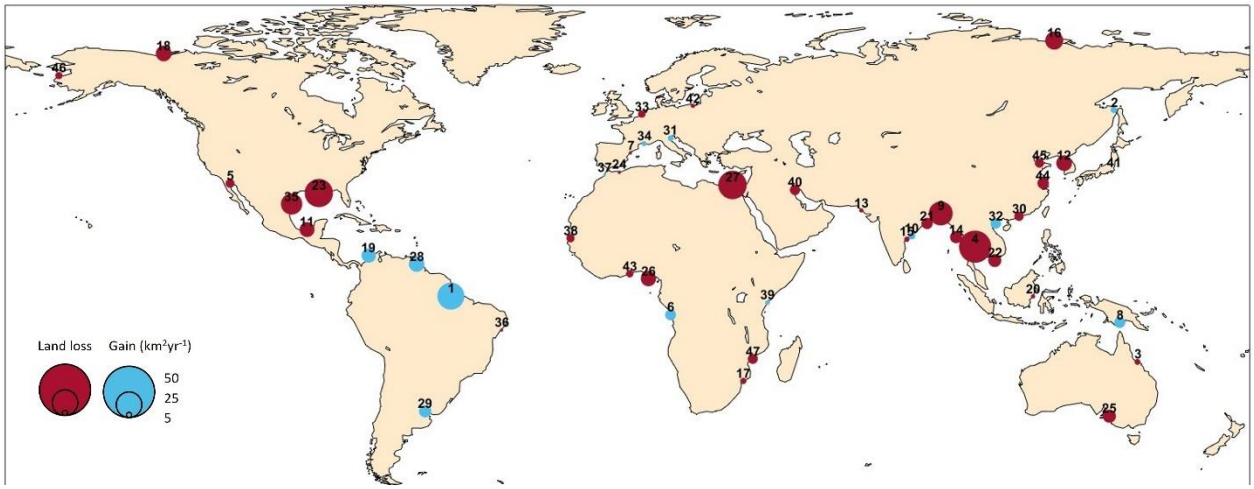

Figure 6.8 Projection of delta area change by 2100 for SSP 3 RCP 4.5 scenario. Each dot represents mean rate of changes (km2/yr). 1 Amazon, 2 Amur, 3 Burdekin, 4 Chao Phraya, 5 Colorado, 6 Congo, 7 Ebro, 8 Fly, 9 GBM, 10 Godavari, 11 Grijalva, 12 Han, 13 Indus, 14 Irrawaddy, 15 Krishna, 16 Lena, 17 Limpopo, 18 Mackenzie, 19 Magdalena, 20 Mahakam, 21 MBB,22 Mekong, 23 Mississippi, 24 Moulouya, 25 Murray, 26 Niger, 27 Nile, 28 Orinoco, 29 Paraná, 30 Pearl, 31 Po, 32 Red, 33 Rhine, 34 Rhône, 35 Rio Grande, 36 São Francisco, 37 Sebou, 38 Senegal, 39 Tana, 40 Tigris Euphrates, 41 Tone, 42 Vistula, 43 Volta, 44 Yangtze, 45 Yellow, 46 Yukon, 47 Zambezi

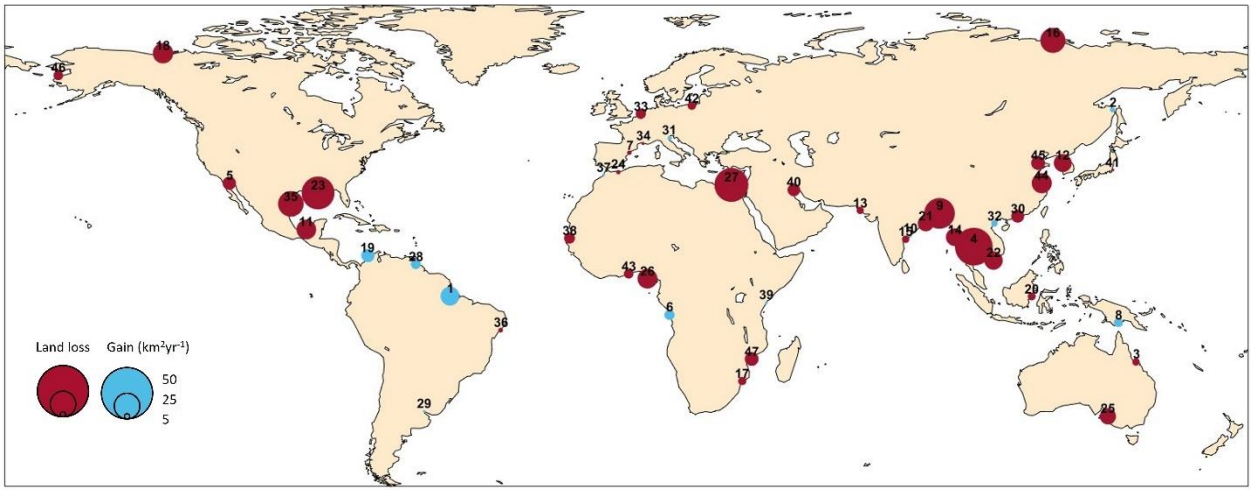

Figure 6.9 Projection of delta area change by 2100 for SSP 3 RCP 8.5 scenario. Each dot represents mean rate of changes (km2/yr). 1 Amazon, 2 Amur, 3 Burdekin, 4 Chao Phraya, 5 Colorado, 6 Congo, 7 Ebro, 8 Fly, 9 GBM, 10 Godavari, 11 Grijalva, 12 Han, 13 Indus, 14 Irrawaddy, 15 Krishna, 16 Lena, 17 Limpopo, 18 Mackenzie, 19 Magdalena, 20 Mahakam, 21 MBB,22 Mekong, 23 Mississippi, 24 Moulouya, 25 Murray, 26 Niger, 27 Nile, 28 Orinoco, 29 Paraná, 30 Pearl, 31 Po, 32 Red, 33 Rhine, 34 Rhône, 35 Rio Grande, 36 São Francisco, 37 Sebou, 38 Senegal, 39 Tana, 40 Tigris Euphrates, 41 Tone, 42 Vistula, 43 Volta, 44 Yangtze, 45 Yellow, 46 Yukon, 47 Zambezi

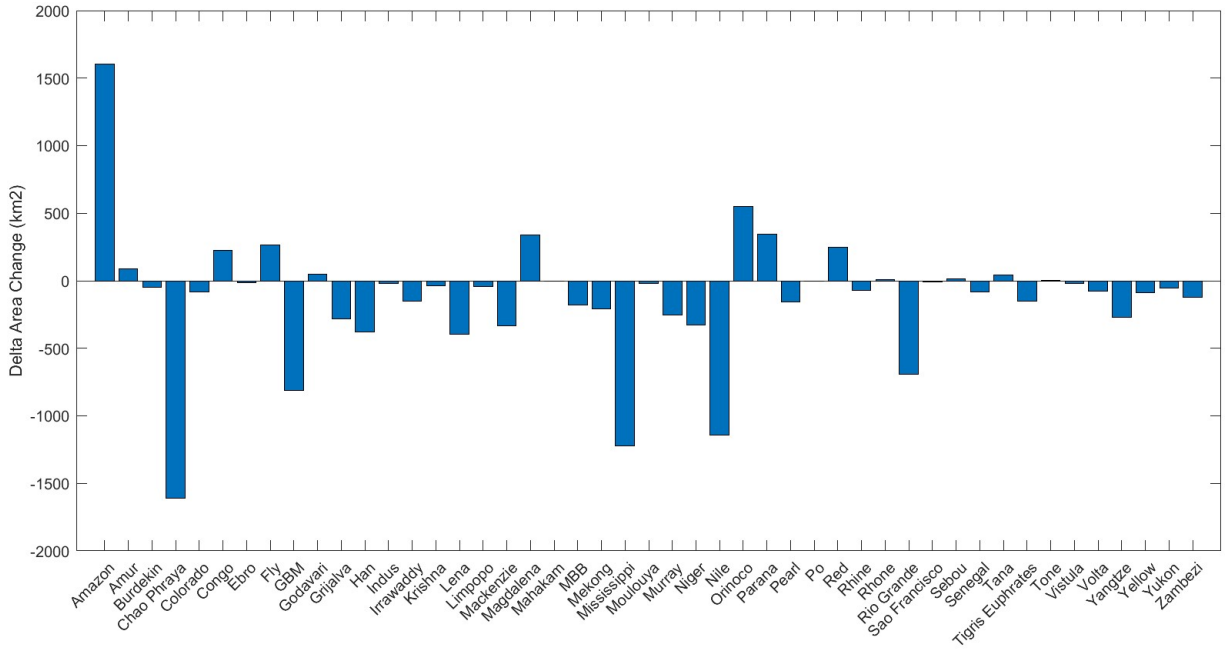

Figure 6.10 projected individual delta area changes for 47 major deltas under SSP 1 RCP 2.6.

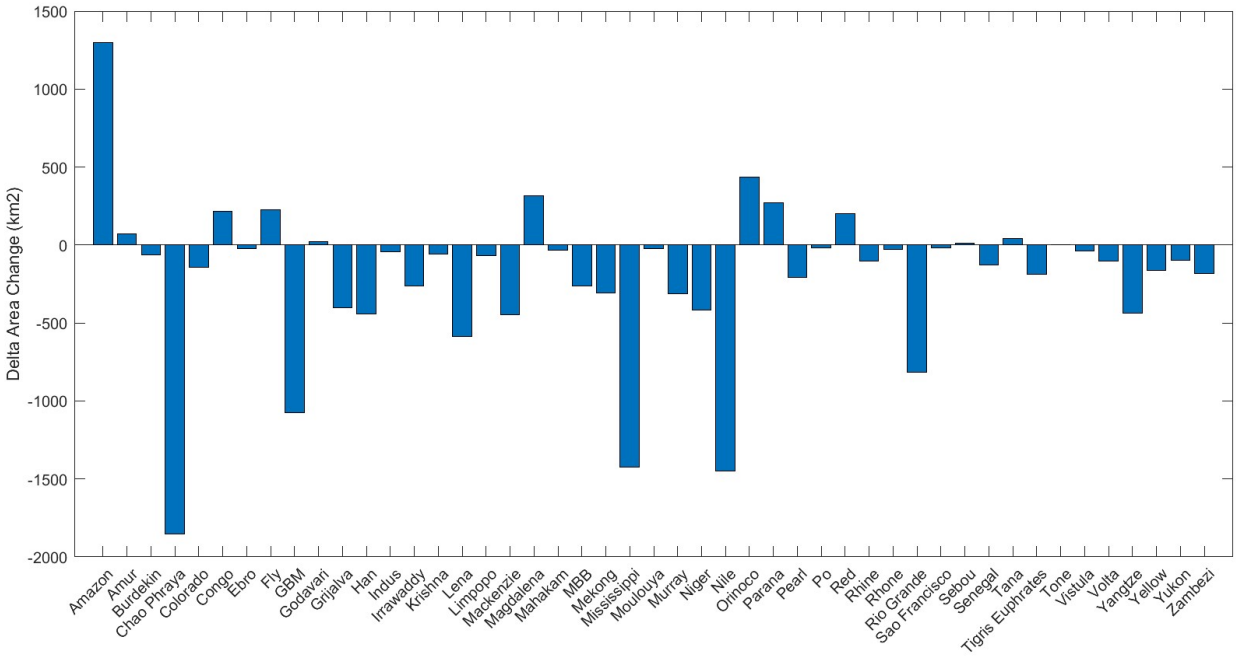

Figure 6.11 projected individual delta area changes for 47 major deltas under SSP 1 RCP 4.5.

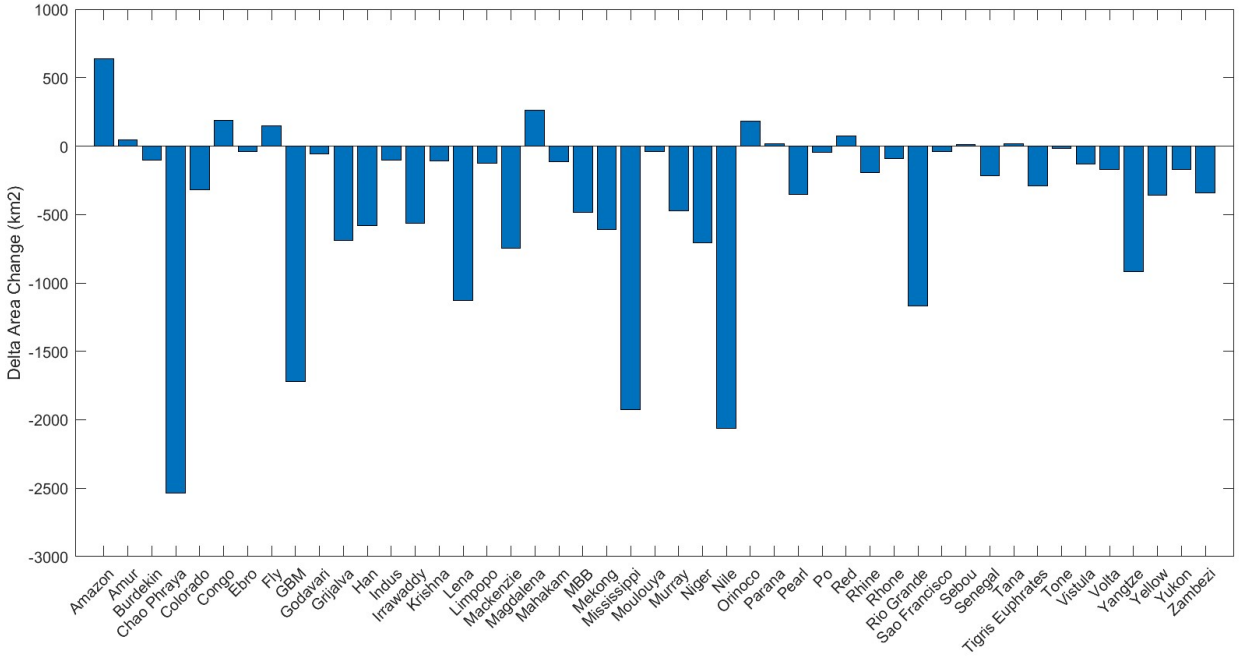

Figure 6.12 projected individual delta area changes for 47 major deltas under SSP 1 RCP 8.5.

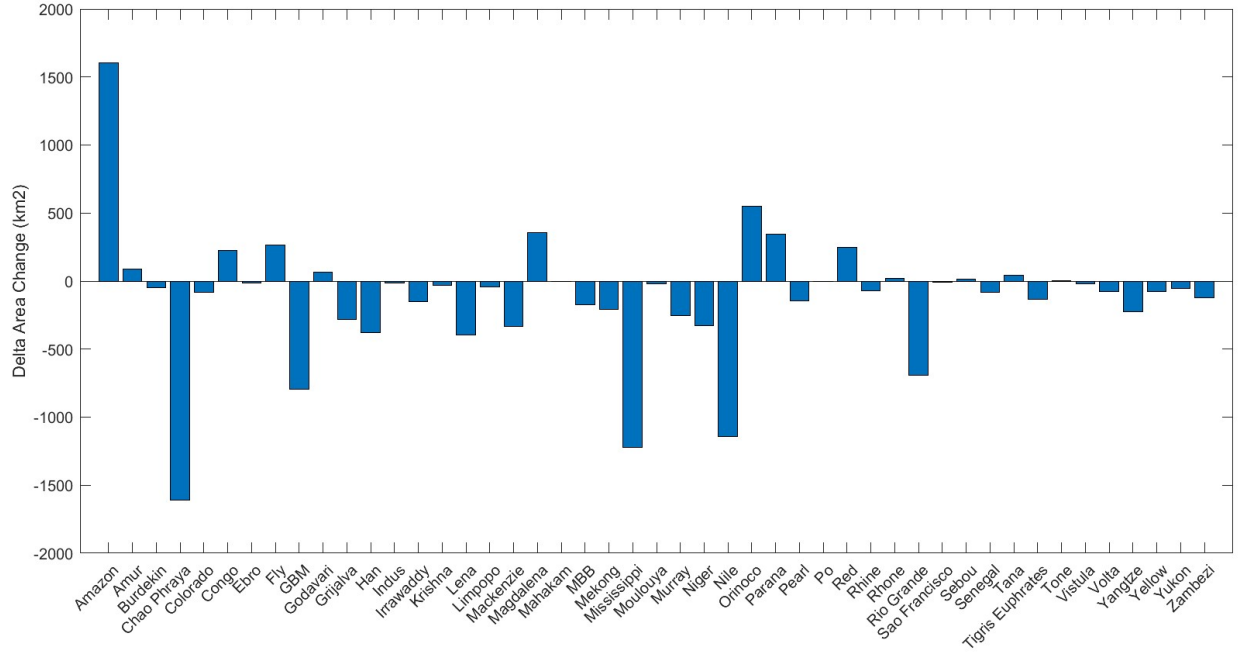

Figure 6.13 projected individual delta area changes for 47 major deltas under SSP 2 RCP 2.6.

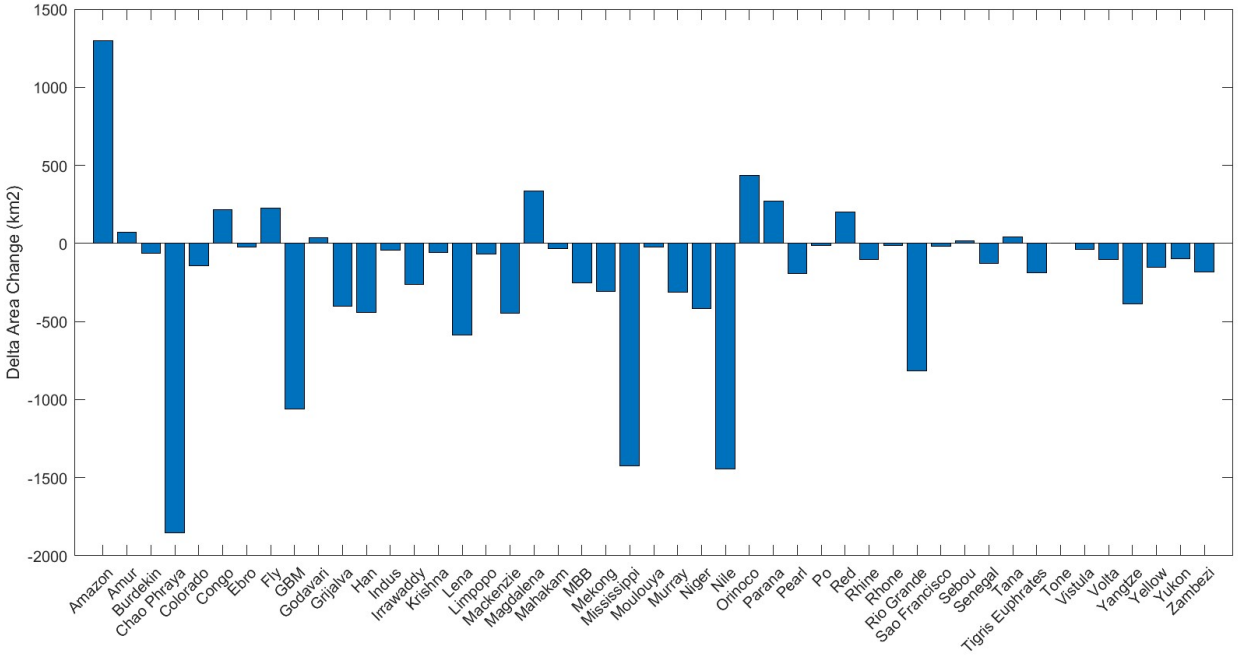

Figure 6.14 projected individual delta area changes for 47 major deltas under SSP 2 RCP 4.5.

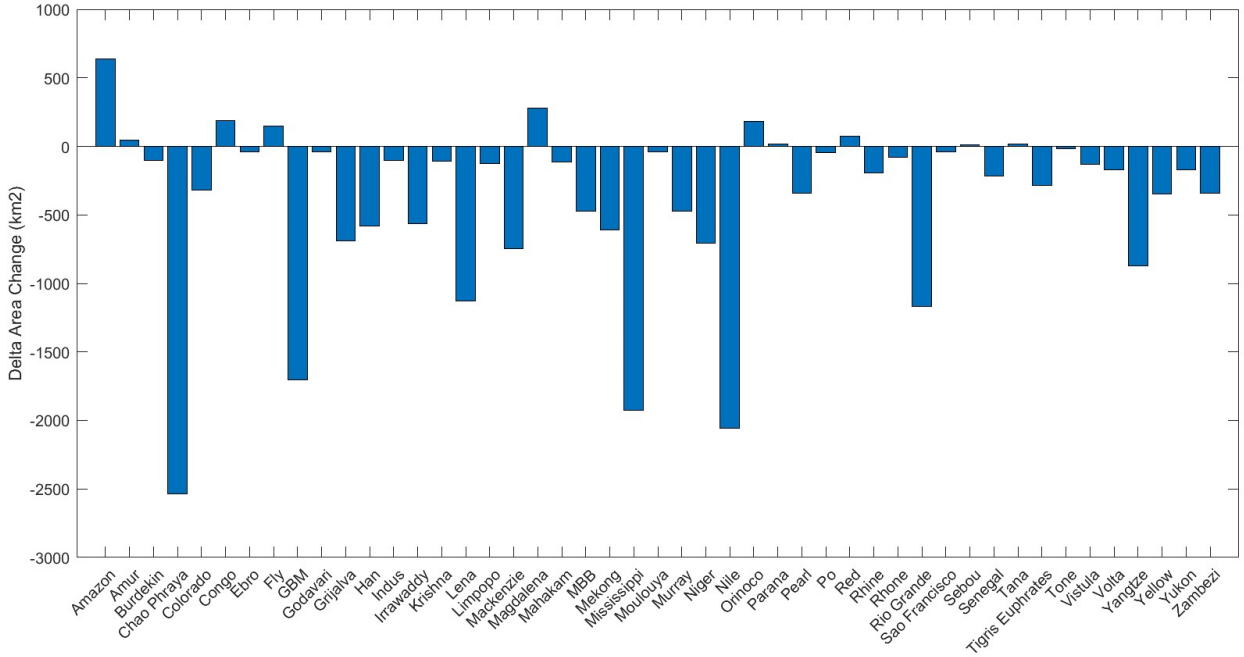

Figure 6.15 projected individual delta area changes for 47 major deltas under SSP 2 RCP 8.5

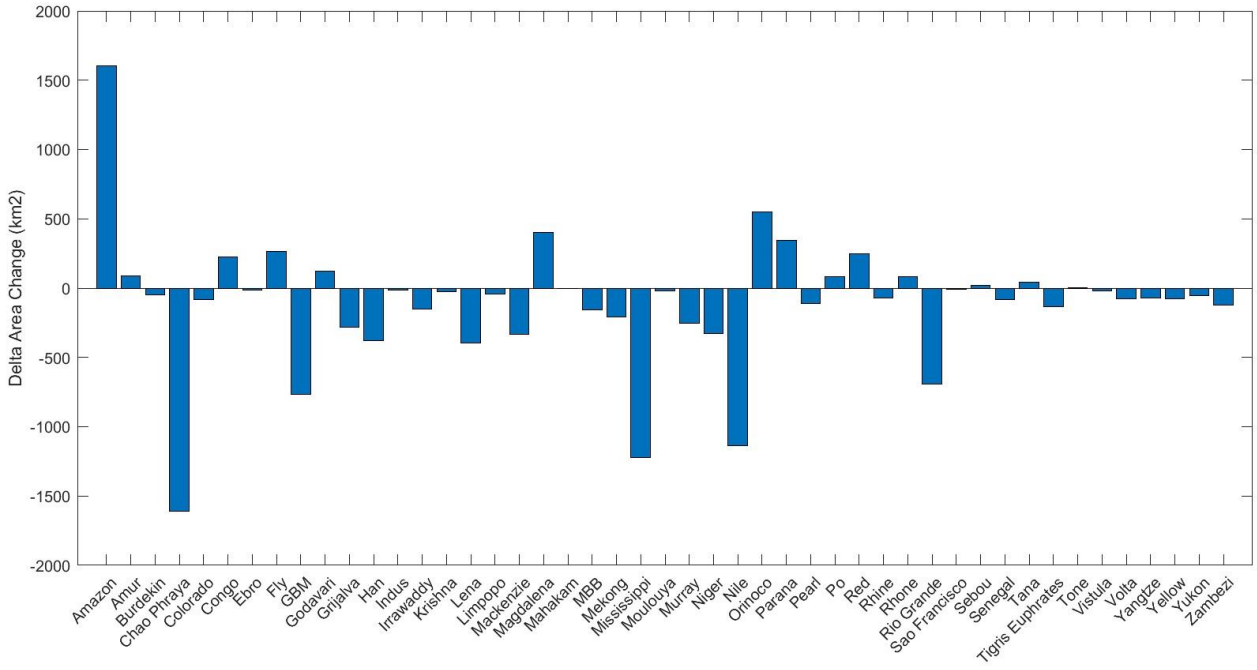

Figure 6.16 projected individual delta area changes for 47 major deltas under SSP 3 RCP 2.6

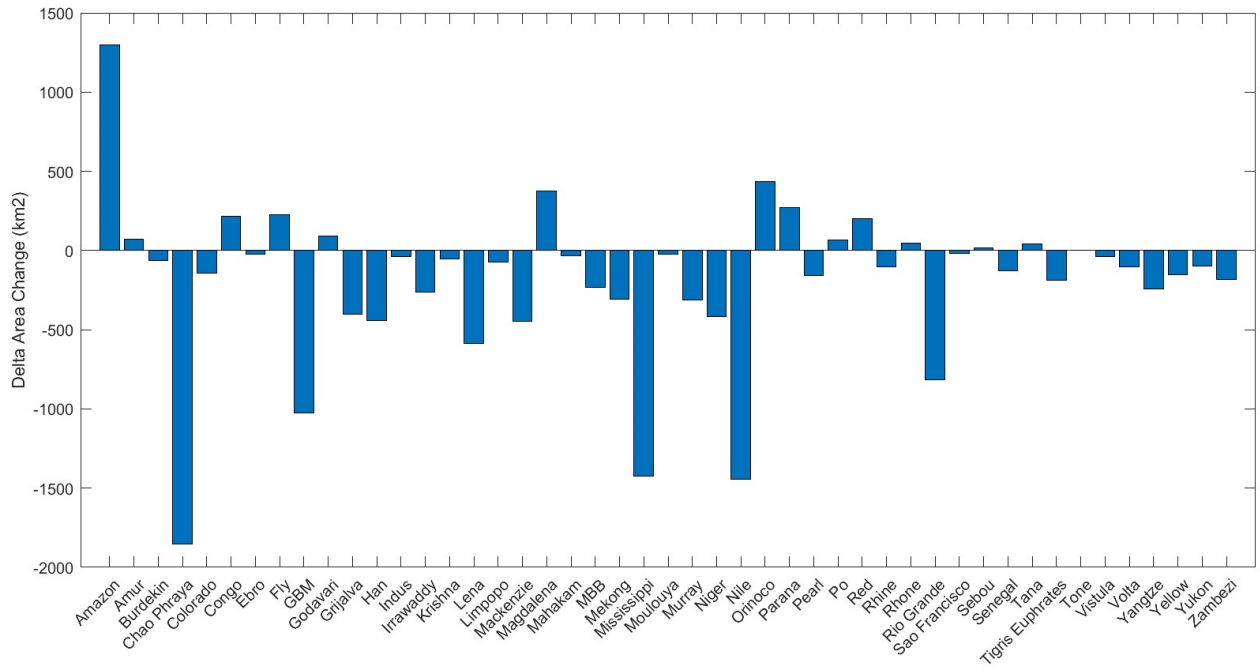

Figure 6.17 projected individual delta area changes for 47 major deltas under SSP 3 RCP 4.5.

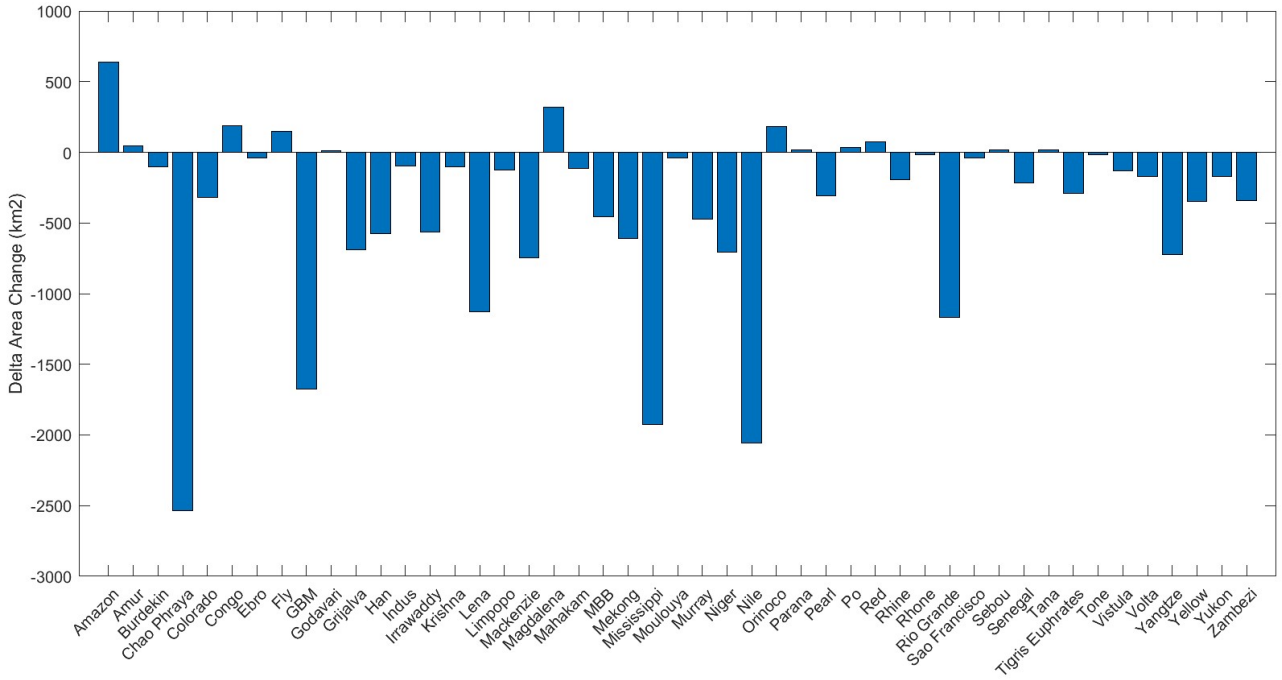

Figure 6.18 projected individual delta area changes for 47 major deltas under SSP 3 RCP 8.5.